ANGLE ESTIMATION USING ADAPTIVE MONOPULSE MUSIC

Thesis

Submitted to

The School of Engineering of the

UNIVERSITY OF DAYTON

In partial fulfillment of the Requirement for

The Degree

Master of Science in Electrical Engineering

By

Edwin Brian Culpepper

UNIVERSITY OF DAYTON

Dayton, OH

May 1998

ANGLE ESTIMATION USING ADAPTIVE MONOPULSE MUSIC

APPROVED BY:

Krishna M. Pasala, Ph.D
Advisory Committee Chairman
Professor,
Electrical & Computer Engineering Department

Mohammed Karim, Ph.D
Committee Member
Chairperson,
Electrical & Computer Engineering Department

Gary A. Thiele, Ph.D
Committee Member
Tait Professor,
Electrical & Computer Engineering Department

Robert Penno, Ph.D
Committee Member
Assistant Professor,
Electrical & Computer Engineering Department

Donald L. Moon, Ph.D
Associate Dean
Graduate Engineering Programs & Research
School of Engineering

Blake Cherrington, Ph.D
Dean, School of Engineering

ABSTRACT

The thesis derives a technique based on an adaptive MUltiple SIgnal Classification (MUSIC) algorithm for the estimation of the angle of arrival of a monopulse system in the presence of mainlobe jamming. A large number of simulations demonstrate that the statistical properties of the algorithm are comparable to those obtained using the Maximum Likelihood Estimator, which is the contemporary method for estimating the angles. The general problem we investigate is the 2-D estimate of arrival angles of a target signal in the presence of main-beam jamming using the monopulse array.

ACKNOWLEDGEMENTS

I want to first thank God from whom all blessings flow, even those we see as trials and hardship instead of challenges and lessons in life.

I would like to express my special thanks to Dr. Krishna M. Pasala for his patience and guidance in the completion of this thesis. In addition, I would also like to thank for their patient and enthusiastic support, everyone that has helped with this work. Many thanks to Erik Blasch for schooling me on MS Word.

It is also very important that I publicly thank my parents, Doris and Cornelius and my wife, special friend and best confidant, Ms. Velma Lynn Culpepper for their never ending patience and understanding. Without their support, this thesis would have not been possible.

TABLES OF CONTENTS

CHAPTER

TABLE OF FIGURES

LIST OF SYMBOLS AND ABBREVIATIONS

AI	Airborne Interceptor
ASLC	Adaptive Sidelobe Canceler
STAP	Space Time Adaptive Processing
PRF	Pulse Repetition Frequency
MLE	Maximum Likelihood Estimator

CHAPTER 1

INTRODUCTION

Angle estimation is a crucial task to be performed by airborne radar. The antenna behind the radome in the nose cone of the aircraft is usually configured to give the four sum and difference beams of a monopulse system. The angle estimation must therefore be based on the signals available in this beam space. Indeed, standard monopulse based angle estimation system proved to be very successful. However, in the presence of main-beam jammer angle estimates based on monopulse are so biased as to be worthless. The objective of the investigation presented in this thesis is to devise a technique that works well even in the presence of jammer.

The standard approach to angle estimation of a signal arriving from an antenna is the Maximum Likelihood Estimator (MLE) [1], which is only one technique of many [2,3,4,5]. Compton [6] explores the use of an adaptive maximum likelihood angle estimator for a monopulse antenna where he relates the bias in the angle estimates to the signal parameters. Compton's approach is based on the original work of Brennan, Reed and Davis [7]. The MLE technique has the advantage of minimal variance with unbiased estimates; however, it requires necessary multidimensional search to determine the angle

1

estimates. A number of authors have developed alternative methodologies: the ESPIRIT algorithm [8] and adaptive arrays [9].

The methodology presented in this thesis is a novel idea for monopulse antenna angle estimation, combining adaptive signal processing for jammer cancellation and MUltiple SIgnal Classification (MUSIC) for high-resolution angle estimation.

A fair amount of research has been directed towards ameliorating the adverse effects due to the presence of main-lobe jammer. Lin and Kretschmer [10] calculated calibration curves from the adapted sum and difference beam weightings and these were used to correct the adapted monopulse estimates. Theil [11] suggested solving detection and angle estimation problems separately, using an adaptive array and super-resolution methods. Nickel [12] derived the correction values for the slope and bias of the adaptive monopulse array. Toulgor and Turner [13] used a two step process of first eliminating the jammer component, using a projection matrix based approach and then carrying out angle estimation. They used the MUSIC [14] method.

The technique presented in this thesis is basically a two step process. The first step consists of estimating and eliminating the jammer component. The technique used for this purpose is different from that used in [13]. The jammer component in each of the beams is eliminated, by using one of the other beams as an "auxiliary beam". The "clean" beamspace signals obtained in this fashion are then used to estimate the angle of arrival using the MUSIC algorithm. It turns out that the MUSIC pseudo-spectrum produces a peak corresponding to the target signal as well as the vestigial jammer. In order to distinguish between these two peaks, least squares analysis is used to estimate the true power associated with these peaks in the MUSIC spectrum. The peak with the higher true

2

power is declared to correspond to the target. An extensive simulation based on the theory presented here is used to evaluate the statistical properties of this new estimator. The estimator yields results comparable to those obtained using the Maximum Likelihood approach but without having to search through the rather complex surfaces associated with the MLE.

The thesis outline is as follows: Chapter 2 reviews the background literature on angle estimation. Section 3 describes the MUSIC algorithm and presents the basic theory behind the algorithm. Section 4 documents the results. Finally Section 5 summarizes the results obtained in this investigation and concludes with future work directions.

CHAPTER 2

ANGLE ESTIMATION

In an airborne interceptor (AI) radar it is necessary to track the movements of one or more targets. Keeping the antenna trained on the target, tracking, requires the sensing of angular pointing errors. In earlier radars a technique called sequential lobing was used to detect these errors. Sequential lobing is performed by sequentially placing the centerline of the beam on one side and the other and above and below the boresight line during reception only. However, because the lobing is sequential, fast changes in the strength of the target echoes can introduce large differences in the returns received through the two lobes and so degrade the tracking accuracy. This problem can be avoided by using an antenna that produces the lobes simultaneously. In modern radars, lobing is accomplished simultaneously by splitting the beam into four overlapping lobes during reception. Because all of the necessary angular tracking information is obtained from one reflected pulse, this technique is called monopulse operation.

This chapter is based largely on information presented in [15] and [16].

2.1 Monopulse Radar Background

Mechanically scanned pencil beams were used in early AI radars used for search and track modes. A single beam can be switched to different positions, and although several beam-switching methods are possible, the most common method of time sharing a single beam is conical scan. In conical scan the beam is moved continuously in a circular pattern, as shown in Figure 1. The target return is amplitude modulated by the beam motion.
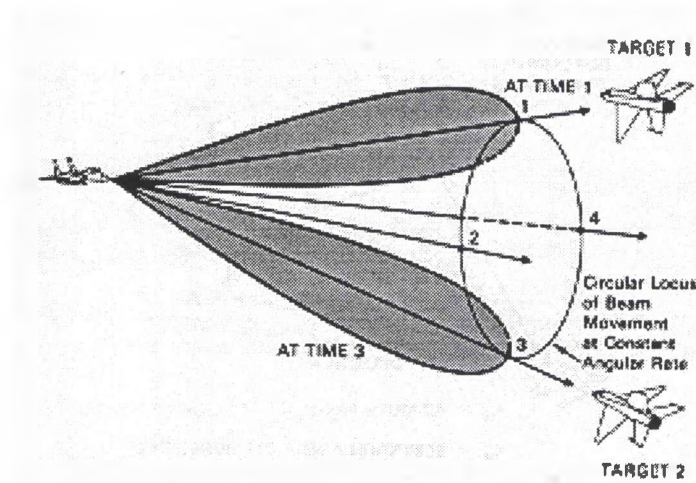
Figure 1. Conical Scan. Courtesy of [16]

The measurements required for tracking can be achieved by moving only the receive beam. However, the usual conical scan implementation moves the transmit beam in space, also. The conical scan frequency is disclosed to the target that, if unfriendly, can use this information to disrupt tracking. Therefore, most military radars no longer use conical scan. Some systems use schemes that move only the receive beam to produce a received signal that resembles that of a conical scan system. The methods are called lobe on receive only or silent lobing.

Conical scan was eventually replaced by monopulse using split apertures which obtained error signals on a single dwell, thus removing target scintillation noise. Mechanically scanned antennas have been replaced by electronically scanned array (ESA) antennas in search allowing track while scan modes of operation. The most common configuration used for tracking is electronic scan with four-aperture monopulse.

The monopulse angle estimation array works very well when there is no jamming present. However, when jamming is present, particularly in the mainlobe of the sum beam of the monopulse output, the performance of the monopulse system is severely degraded. Indeed, the system declares the jammer bearing to be that of the target bearing. Thus, for reliable angle estimation, the monopulse output must be rid of the jammer component. This must be done adaptively. Recently it was found that multiple apertures and beam clusters could be used adaptively to reduce main beam jamming, and that with space-time adaptive processing (STAP), targets could be detected in clutter. This makes possible the detection of low flying aircraft and slowly moving ground vehicles from almost all angles of attack. A penalty for using the spatial degrees of freedom for interference reduction is that the resulting beam amplitude and phase are distorted which in turn makes angle estimation in the usual way impossible.

Tracking is done to improve the estimates of target position and velocity relative to those that can be provided in the search mode. During tracking, in angle, range, or doppler, the target response must be measured at two or more positions, again in angle, range or doppler. The two measurements can be achieved by using a single beam, time-shared at

various positions (sequential lobing or conical scan) or by using multiple simultaneous beams (monopulse operation).

Angle measurements are made using either amplitude comparison or phase comparison. Amplitude comparison is illustrated in Figure 2. Two similar beams are produced, that are separated in angle by a fraction of a beamwidth. The angle at which the amplitudes of the two beams are equal is called the angle zero reference point. The voltages produced in the two beams by a point source we denote as v1 and v2. A calibration curve of voltage ratio (v1/v2) in dB verses the angle that is independent of target signal strength is used to determine angle error. When (v1/v2) is measured, the angle away from boresight is determined using the calibration curve. The angle-off measurement is used to correct the antenna position to drive the angle-off to zero.
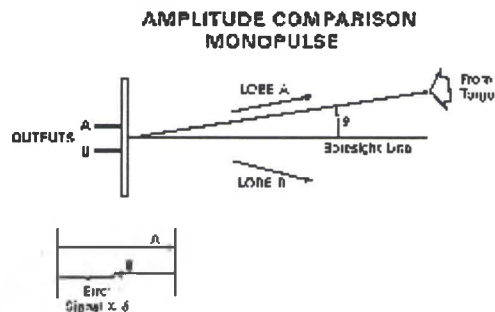
Figure 2. Amplitude Comparison. Courtesy of [16]

The most common antenna configuration in airborne systems is the monopulse planar array. Monopulse indicates the ability to derive angle error from a single pulse. A planar array is made up of a number of radiating slots cut in a plane surface. The planar array is subdivided into quadrants that are fed by a microwave sum and difference network. First consider a planar array subdivided into two sections: A and B, as shown in Figure 3. The microwave sum and difference network creates, from the two lobes A and B, two beams

7

sum (Σ) beam and difference (Δ) beam. The Δ = A + B and Σ = A - B. The gain and beamwidth of both the Δ and Σ patterns are determined by the total aperture, (A + B). The null of the Δ pattern occurs at the peak of the Σ pattern.
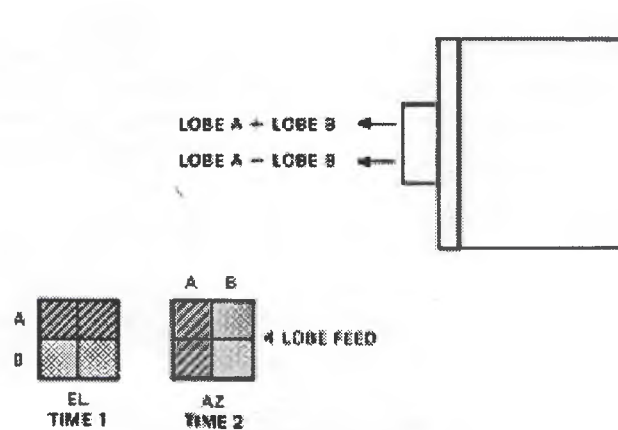
Figure 3. Planner Array. Courtesy of [16]

A calibration curve can be used that is analogous to the amplitude comparison system. The ratio Δ/Σ is used, which is independent of target strength. The magnitude of the Δ pattern is symmetrical about zero angle error but is in phase with the sum channel on one side of zero and 180 out of phase on the other. By subtracting the output of one feed from the output of the other, an angular tracking error signal is produced. The sum of the two outputs is used for tracking.

Figure 4 shows a four-quadrant monopulse antenna that can track in azimuth and elevation. By dividing the antenna into quadrants, so that the feed design produces four lobes instead of just two, simultaneous lobing can be achieved in both azimuth and elevation. These four antenna ports are connected to a manifold, a device for combining the receiver RF signals, to obtain sum (Σ), difference-azimuth (Δaz), difference-elevation (Δel) and, difference-difference ($\Delta\Delta$) beam outputs. The four beams, Δaz, Δel, $\Delta\Delta$, and Σ,

8

each use the entire aperture. Δaz = A-B+C-D Δel = A+B-C-D, $\Delta\Delta$ = A-B-C+D, and Σ = A+B+C+D. The antenna pattern for the Δaz and Δel ports will exhibit a null directly between the beams while the $\Delta\Delta$ port will exhibit two nulls. The patterns for the sum port however, will exhibit a peak directly center the beams. This makes pencil-beam tracking and/or angle measurement with very high precision possible.

Traditional monopulse, using amplitude comparison, duplicates sequential lobing with simultaneously formed lobes A, B, C and D. Because the lobes point in slightly different directions, if a target is not on the boresight line of the antenna, the amplitude of the return received through one lobe differs from the amplitude of the return simultaneously received through the other lobe. The difference is proportional to the angular error.
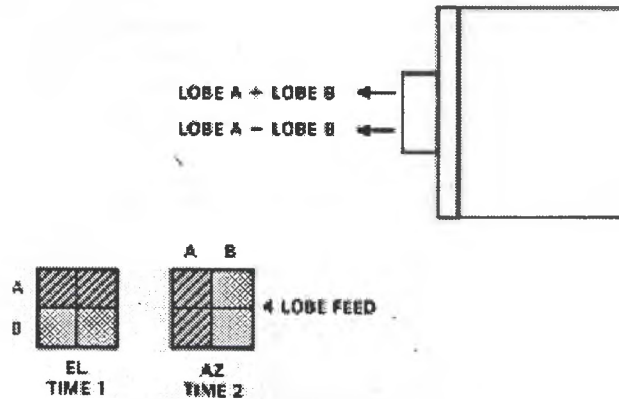
Figure 4. Four-Quadrant Monopulse Antenna. Courtesy of [16]

By continuously sensing the tracking errors with monopulse operation and continuously correcting the pointing direction of the antenna so as to reduce the errors to zero, the antenna can be made to follow the movement of a target with extreme precision.

A monopulse radar measures the azimuth and elevation angles of the line-of-sight vector from the aircraft to the target. The basic vector geometry defining the azimuth angle (α)

9

and elevation (ε) angle are shown below in Figure 5. Here, the azimuth angle is defined to be the angle between a vector pointing along the antenna frame y-axis and the line-of-sight vector. The elevation angle is defined to be the angle between a vector pointing along the antenna frame z-axis and the line-of-sight vector. The antenna frame is defined in detail in the next section of this thesis.
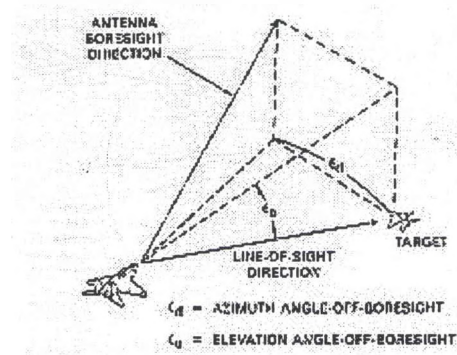
Figure 5. Vector Geometry. Courtesy of [16]

Many airborne radar systems include a monopulse radar mode. In operation, the monopulse processor measures the azimuth and elevation angles for target tracking. The angles α and ε are known only after operator designates target range Doppler cell.

2.2 Geometry of Monopulse Radar Azimuth and Elevation Angle Measurements

The geometry defining the azimuth angle (α) and elevation (ε) angle is shown in Figure 6 below.
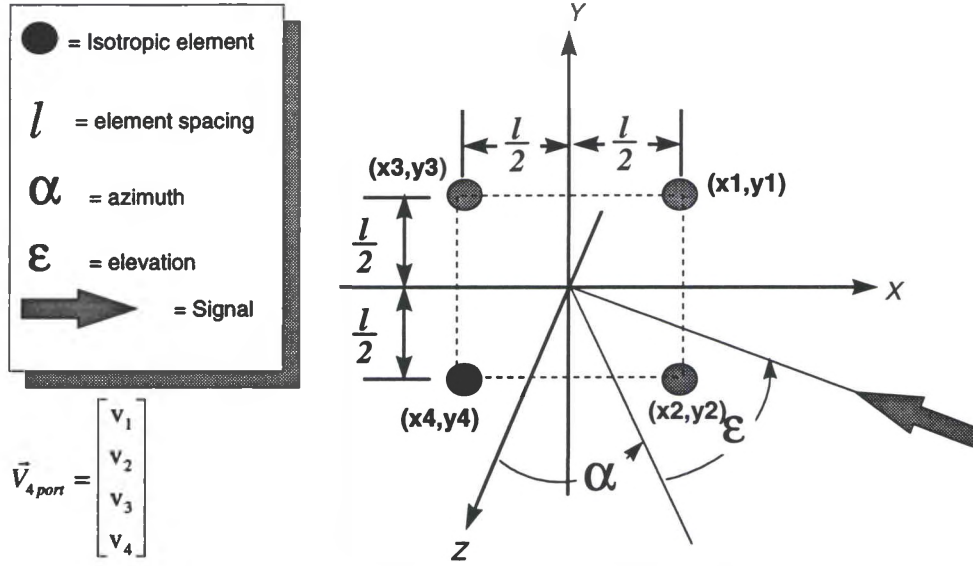
Figure 6. Geometry of Four-Port Monopulse Array.

Consider the unit vectors $\mathbf{u}_{py}^a$ and $\mathbf{u}_{pz}^a$ which point in y^a and z^a directions, respectively. These vectors are expressed in the antenna coordinates as

$$\mathbf{u}_{py}^a = [\ 0\ \ 1\ \ 0\ ]^T \tag{1}$$

$$\mathbf{u}_{pz}^a = [\ 0\ \ 0\ \ 1\ ]^T \tag{2}$$

and may be converted to the navigation frame by employing coordinate transformations:

$$\mathbf{u}_{py}^n = C_b^n\, C_a^b\, \mathbf{u}_{py}^a = C_a^n\, \mathbf{u}_{py}^a \tag{3}$$

$$\mathbf{u}_{pz}^n = C_b^n\, C_a^b\, \mathbf{u}_{pz}^a = C_a^n\, \mathbf{u}_{pz}^a \tag{4}$$

The relationship between α and ε (quantities measured by the radar) and the unit vectors

of interest are given by:

$$\cos(\alpha) = (\mathbf{u}_p^n)^T\, \mathbf{u}_{py}^n \tag{5}$$

$$\cos(\varepsilon) = (\mathbf{u}_p^n)^T\, \mathbf{u}_{pz}^n \tag{6}$$

Solving for α and ε yields

$$\alpha = \cos^{-1} [(\mathbf{u}_p^n)^T\, \mathbf{u}_{py}^n] \tag{7}$$

$$\varepsilon = \cos^{-1} [(\mathbf{u}_p^n)^T\, \mathbf{u}_{pz}^n] \tag{8}$$

where both α and ε lie in the interval $[-\pi/2,\ \pi/2]$ radians.

11

A CW signal incident on this array from azimuth angle α and elevation angle ε will produce the following element voltages

$$\vec{V}_k = \vec{A}_k\, u_k \tag{9}$$

$$\vec{A}_k = \begin{bmatrix} f_1(\alpha_k,\varepsilon_k)\, e^{j\beta_{kx}x_1}\, e^{j\beta_{ky}y_1} \\ f_2(\alpha_k,\varepsilon_k)\, e^{j\beta_{kx}x_2}\, e^{j\beta_{ky}y_2} \\ f_3(\alpha_k,\varepsilon_k)\, e^{j\beta_{kx}x_3}\, e^{j\beta_{ky}y_3} \\ f_4(\alpha_k,\varepsilon_k)\, e^{j\beta_{kx}x_4}\, e^{j\beta_{ky}y_4} \end{bmatrix} \tag{10}$$

$$\beta_{kx} = \qquad k = 1, 2, \ldots, K \tag{11}$$
$$\beta_{ky} = \qquad k = 1, 2, \ldots, K \tag{12}$$
$$u_k = a_k(t)\, e^{j\omega_k t} \tag{13}$$

$$\vec{V}_k = \begin{bmatrix} f_1(\alpha_k,\varepsilon_k)\, e^{j\beta_{kx}x_1}\, e^{j\beta_{ky}y_1} \\ f_2(\alpha_k,\varepsilon_k)\, e^{j\beta_{kx}x_2}\, e^{j\beta_{ky}y_2} \\ f_3(\alpha_k,\varepsilon_k)\, e^{j\beta_{kx}x_3}\, e^{j\beta_{ky}y_3} \\ f_4(\alpha_k,\varepsilon_k)\, e^{j\beta_{kx}x_4}\, e^{j\beta_{ky}y_4} \end{bmatrix} a_k(t)\, e^{j\omega_k t} \qquad k = 1, 2, \ldots, K \tag{14}$$

$$\vec{V}_{4port} = \vec{V}_1 + \vec{V}_2 + \ldots + \vec{V}_K \tag{15}$$

$$\vec{V}_{4port} = \begin{bmatrix} v_1 \\ v_2 \\ v_3 \\ v_4 \end{bmatrix} = [\ \vec{A}_1 \quad \vec{A}_2\ ] \cdot \begin{bmatrix} u_1 \\ u_2 \end{bmatrix} + \vec{v}_{noise} \tag{16}$$

Equations (15) and (16) represent the Conventional Four Port Signal Model used in our analysis whereas equation (18) and Figure 7 show the Monopulse Signal model which is obtained from (16) through the monopulse transformation matrix M, defined by

$$M = \begin{bmatrix} 1 & 1 & 1 & 1 \\ 1 & 1 & -1 & -1 \\ 1 & -1 & 1 & -1 \\ 1 & -1 & -1 & 1 \end{bmatrix} \tag{17}$$
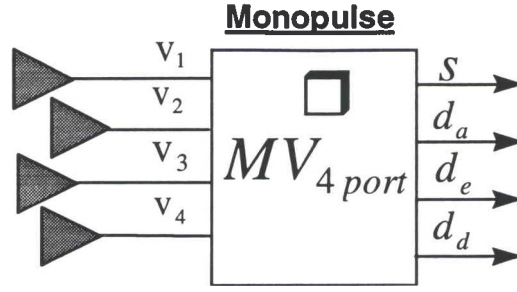
Figure 7. Monopulse Signal Model.

$$\vec{V}_{mp} = \begin{bmatrix} s \\ d_a \\ d_e \\ d_d \end{bmatrix} = \begin{bmatrix} v_1 + v_2 + v_3 + v_4 \\ v_1 + v_2 - v_3 - v_4 \\ v_1 - v_2 + v_3 - v_4 \\ v_1 - v_2 - v_3 + v_4 \end{bmatrix} = M\vec{V}_{4port} = \begin{bmatrix} 1 & 1 & 1 & 1 \\ 1 & 1 & -1 & -1 \\ 1 & -1 & 1 & -1 \\ 1 & -1 & -1 & 1 \end{bmatrix} \cdot \begin{bmatrix} v_1 \\ v_2 \\ v_3 \\ v_4 \end{bmatrix} \qquad (18)$$

2.3 Targeting with Monopulse Measurements

In general, targeting algorithms need three pieces of information to compute a target's location, namely range, range rate (doppler), and height above the target. As shown in Figure 8, the intersection of the sphere of constant range, cone of constant range rate (centered about the aircraft velocity vector), and the plane of constant height above target defines the location of the target.
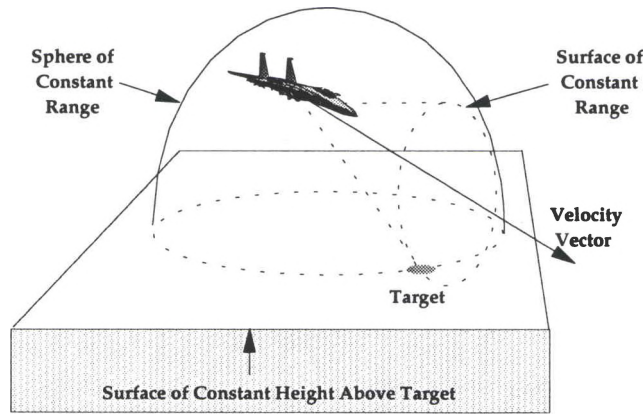
Figure 8. Range-Doppler Target Location Geometry.

13

Range and range rate are inherently measured and stored for each cell in a Doppler processed SAR image. The height above target, can be computed from the range measurement and the precise angle measurements of a monopulse radar. Recall that monopulse radar is capable of measuring the azimuth angle, α, and the elevation angle ε. Similar to the SAR measurements, the monopulse radar measurements are also corrupted by a number of errors. As a result, they may be expressed as the sum of the true value and the measurement errors. For an electronically scanned array antenna (ESA), which we now assume, the measured azimuth angle, denoted

$\hat{\alpha}$ and, elevation angle, denoted $\hat{\varepsilon}$, are modeled by the following equations:

$$\hat{\alpha} = \alpha + error \tag{19}$$

$$\hat{\varepsilon} = \varepsilon + error \tag{20}$$

Potential errors in the azimuth and elevation angle measurement, which are not modeled here, include atmospheric bending effects, **temperature errors**, **mechanically steering errors**, **flexure errors**, **positioning errors**, phase quantization and phase shifter errors, monopulse slope and, **quantization errors**.

CHAPTER 3

ADAPTIVE MONOPULSE MUSIC

In this chapter, the theory pertaining to the new technique, "Adaptive Monopulse MUSIC" is discussed. This technique has three salient features:

1) The jammer in each of the sum and difference beams corresponding to the range bin under test estimated and subtracted. This jammer estimation is based on the measurements of signal in the adjacent range bins which is presumed to be target free but whose clutter is correlated to the jammer in the range bin under test. This process results in a substantial reduction in jammer but does not eliminate it altogether. Section 3.1 discusses this issue.

2) Using the outputs of these adapted monopulse beams, the angles of arrival are estimated using the MUSIC algorithm. Since the jammer is not eliminated, the MUSIC algorithm produces a peak in the pseudo spectrum corresponding to the jammer as well as the target signal.

3) Sorting of the peaks of the pseudo spectrum into the target peak and jammer peak is carried out next. This is accomplished by estimating the actual powers associated with the peak using lease squares technique. The peak corresponding to the higher power is declared to be the target.

3.1 Adaptive Monopulse

The monopulse array works very well when there is no jamming present. However as shown in Figure 9, when jamming is present particularly in the mainlobe of the sum beam of the monopulse output, the performance of the monopulse system is severely degraded due to the distortion of the adapted sum and difference beams. Indeed, the system declares the jammer bearing to be that of the target bearing. Thus, for reliable angle estimation, the monopulse output must be rid of the jammer component. This must be done adaptively. This is accomplished as follows, using the concept of the adaptive sidelobe canceler.
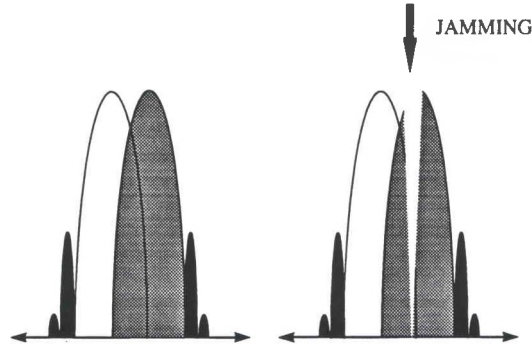
Figure 9. Distortion of Monopulse Antenna Pattern (Jamming).

We define $\vec{V}_{AMP}$ the adaptive monopulse output as follows:

$$\vec{V}_{AMP} = \begin{bmatrix} S \\ D_a \\ D_e \\ D_d \end{bmatrix} = \vec{V}_{mp} - \vec{V}_{wt} = \begin{bmatrix} s \\ d_a \\ d_e \\ d_d \end{bmatrix} - \begin{bmatrix} w_{as}d_e \\ w_{ad}d_d \\ w_{es}d_d \\ w_{ed}s \end{bmatrix} = \vec{V}_{mp} - W_{AMP}M_{AMP}\vec{V}_{mp} \qquad (21)$$

16

$$\vec{V}_{mp} = \begin{bmatrix} s \\ d_a \\ d_e \\ d_d \end{bmatrix} \tag{22}$$

$$\vec{V}_{wt} = \begin{bmatrix} w_{as}d_e \\ w_{ad}d_d \\ w_{es}d_d \\ w_{ed}s \end{bmatrix} \tag{23}$$

$$M_{AMP} = \begin{bmatrix} 0 & 0 & 1 & 0 \\ 0 & 0 & 0 & 1 \\ 0 & 0 & 0 & 1 \\ 1 & 0 & 0 & 0 \end{bmatrix} \tag{24}$$

$$W_{AMP} = \begin{bmatrix} w_{as} & 0 & 0 & 0 \\ 0 & w_{ad} & 0 & 0 \\ 0 & 0 & w_{es} & 0 \\ 0 & 0 & 0 & w_{ed} \end{bmatrix} \tag{25}$$

The elements of this vector are defined as follows:

$$S = s - w_{as} \times d_e \tag{26}$$
$$D_a = d_a - w_{ad} \times d_d \tag{27}$$
$$D_e = d_e - w_{es} \times d_d \tag{28}$$
$$D_d = d_d - w_{ds} \times s \tag{29}$$
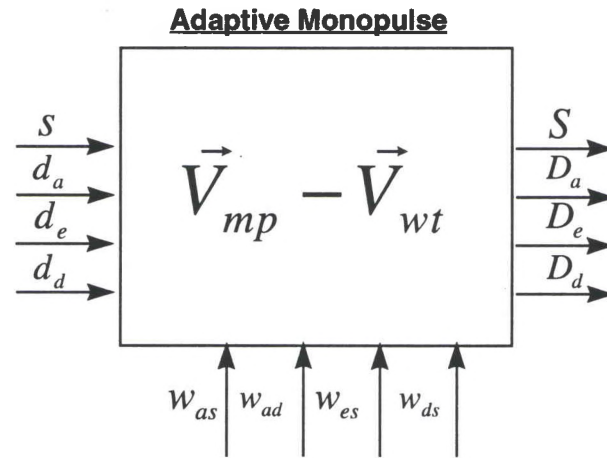
Figure 10. Adaptive Monopulse Signal Model.

The weights, w_{as}, w_{ad}, w_{es}, and w_{ds} are chosen in such a way that the component of the jammer power in the monopulse output is minimized. The signal model is shown in Figure 10.

To compute these weights let us consider the mechanics of weight computation. As an example, let us consider the determination of w_{as} which helps null out the jammer from the sum output, s. For this purpose we use the output of the delta elevation beam d_e as an auxiliary. Since the target is in the vicinity of the null, the difference beam output d_e has only a small component of the target signal and largely consists of jamming. The weight w_{as} is so chosen that $w_{as} \times d_e$ cancels the jammer component of the sum beam output to the greatest extent possible. To the extent there is a signal component in d_e, however small, it results in signal cancellation. In the context of radar, it is possible to avoid this signal cancellation completely. This is accomplished by using the outputs of range bins adjoining the target range bin. The jammer signal in these range bins is approximately the same as that in the target range bin. Thus, the quantity to be minimized is the residual power:

$$\mathrm{E}\left[\,|S_j|^2\right] = \mathrm{E}\left[\,(s_j - w_{as} \times d_{ej})\,(s_j^* - w_{as}^* \times d_{ej}^*)\,\right] \tag{30}$$

This is a straightforward problem and the solution is given by:

$$w_{as} = \frac{\mathrm{E}[\,s_j \times d_{ej}^*]}{\mathrm{E}[\,|d_{ej}|^2]} \tag{31}$$

The minimum residual power is given by:

$$P_{\text{residual}} = \mathrm{E}\left[\,|s_j|^2 - w_{as} \times d_{ej} \times s_j^* - w_{as}^* \times s_j \times d_{ej}^* + |w_{as}|^2 \times |d_{ej}|^2\,\right]$$

$$P_{residual} = E\left[\,|\,s_j\,|^2\,\right] - 2 \times \text{Re}\left\{\,E\left[w_{as} \times d_{ej} \times s_j^{*}\right]\right\} + |\,w_{as}\,|^2 \times |\,d_{ej}\,|^2 \tag{32}$$

Substituting for w_{as} from above, we get

$$P_{residual} = E\left[\,|\,s_j\,|^2\,\right] - 2 \times \text{Re}\left\{\frac{E[\,s_j \times d_{ej}^{*}]}{E[\,|d_{ej}|^2]} \times E\left[d_{ej} \times s_j^{*}\right]\right\} + \left|\frac{E[\,s_j \times d_{ej}^{*}]}{E[\,|d_{ej}|^2]}\right|^2 \times |\,d_{ej}\,|^2$$

$$= E\left[\,|\,s_j\,|^2\,\right] - 2 \times \frac{|\,E[s_j \times d_{ej}^{*}]\,|^2}{E[\,|d_{ej}|^2]} + \frac{|\,E[s_j \times d_{ej}^{*}]\,|^2}{E[\,|d_{ej}|^2]}$$

$$= E\left[\,|\,s_j\,|^2\,\right] + \frac{|\,E[s_j \times d_{ej}^{*}]\,|^2}{E[\,|d_{ej}|^2]} \tag{33}$$

Thus, the jammer power $E\left[\,|\,s_j\,|^2\,\right]$ is reduced by the factor $|\,E[s_j \times d_{ej}^{*}]\,|^2\,/\,E[\,|d_{ej}|^2]$.

The residual power may be close to zero but not necessarily zero. The weights are given by,

$$w_{as} = \frac{E\left[s_{(jam+noise)}d_{e(jam+noise)}^{*}\right]}{E\left[\,|d_{e(jam+noise)}|^2\right]} \tag{34}$$

$$w_{ad} = \frac{E\left[d_{a(jam+noise)}d_{d(jam+noise)}^{*}\right]}{E\left[\,|d_{d(jam+noise)}|^2\right]} \tag{35}$$

$$w_{es} = \frac{E\left[s_{(jam+noise)}d_{a(jam+noise)}^{*}\right]}{E\left[\,|d_{a(jam+noise)}|^2\right]} \tag{36}$$

$$w_{ds} = \frac{E\left[d_{d(jam+noise)}s_{(jam+noise)}^{*}\right]}{E\left[\,|s_{(jam+noise)}|^2\right]} \tag{37}$$

Figure 11. Weight Computation.

$$\vec{V}_{AMP} = \begin{bmatrix} S \\ D_a \\ D_e \\ D_d \end{bmatrix} = \vec{V}_{mp} - \vec{V}_{wt} = \begin{bmatrix} s \\ d_a \\ d_e \\ d_d \end{bmatrix} - \begin{bmatrix} w_{as}d_e \\ w_{ad}d_d \\ w_{es}d_d \\ w_{ed}s \end{bmatrix}$$

where,

$$\mathrm{E}[\ |s_{(jam+noise)}|^2] = \mathrm{E}\ [\ (s^*_{(jam+noise)} - w^*_{as}d^*_{e(jam+noise)})\ (s_{(jam+noise)} - w_{as}d_{e(jam+noise)})\ ] \tag{38}$$

and,

$$\vec{V}_{jam+noise} = \begin{bmatrix} s_{(jam+noise)} \\ d_{a(jam+noise)} \\ d_{e(jam+noise)} \\ d_{d(jam+noise)} \end{bmatrix} \tag{39}$$

20
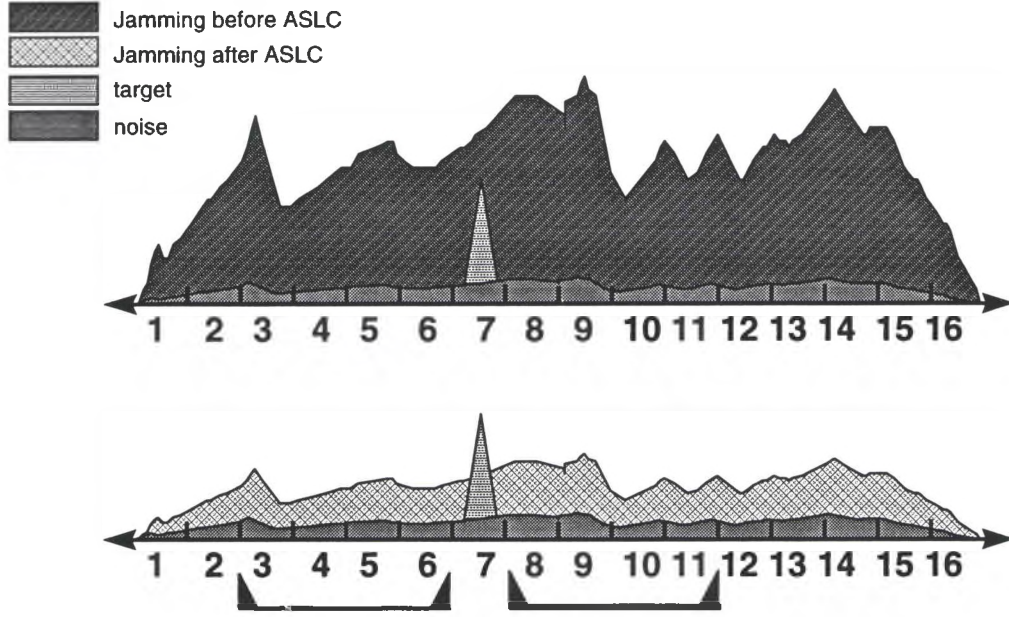
Figure 12. Data Samples for $\vec{V}_{jam + noise}$.

The adaptive monopulse output is given by

$$S = s - w_{as} \times d_{e(jam + noise)} \tag{40}$$

$$D_a = d_a - w_{ad} \times d_{d(jam + noise)} \tag{41}$$

$$D_e = d_e - w_{es} \times d_{d(jam + noise)} \tag{42}$$

$$D_d = d_d - w_{ds} \times s_{(jam + noise)} \tag{43}$$

These equations may be expressed compactly using matrix notation as follows.

$$\vec{V}_{adap} = \vec{V}_{mono} - \vec{V}_{corr} + \vec{V}_{noise} \tag{44}$$

Where the correlation voltages $\vec{V}_{corr}$ are given by,

$$\vec{V}_{corr} = \begin{bmatrix} w_{as} \times d_{e(jam + noise)} \\ w_{ad} \times d_{d(jam + noise)} \\ w_{es} \times d_{d(jam + noise)} \\ w_{ds} \times s_{(jam + noise)} \end{bmatrix} = W_{adap} M_{adap} \vec{V}_{(jam + noise)} \tag{45}$$

where,

21

$$
W_{adap} = \begin{bmatrix} w_{as} & 0 & 0 & 0 \\ 0 & w_{ad} & 0 & 0 \\ 0 & 0 & w_{es} & 0 \\ 0 & 0 & 0 & w_{ds} \end{bmatrix} \quad \text{and} \quad M_{adap} = \begin{bmatrix} 1 & -1 & 1 & -1 \\ 1 & -1 & -1 & 1 \\ 1 & -1 & -1 & 1 \\ 1 & 1 & 1 & 1 \end{bmatrix}
$$

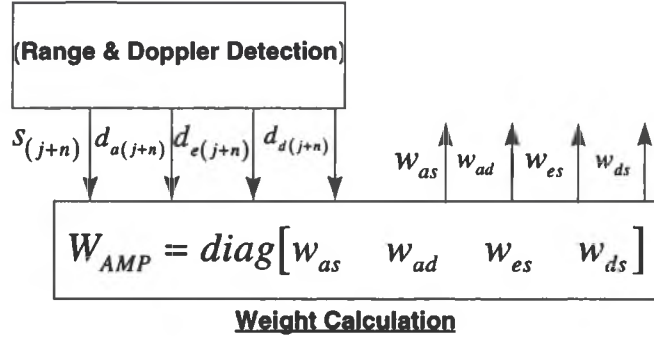or written as:

$$
\vec{V}_{AMP} = \begin{bmatrix} S \\ D_a \\ D_e \\ D_d \end{bmatrix} = \vec{V}_{mp} - \vec{V}_{wt} = \begin{bmatrix} s \\ d_a \\ d_e \\ d_d \end{bmatrix} - \begin{bmatrix} w_{as}d_e \\ w_{ad}d_d \\ w_{es}d_d \\ w_{ed}s \end{bmatrix} = \vec{V}_{mp} - W_{AMP}M_{AMP}\vec{V}_{mp} \tag{46}
$$

$$
\vec{V}_{AMP} = \begin{bmatrix} S \\ d_a \\ d_e \\ d_d \end{bmatrix} - \begin{bmatrix} w_{as} & 0 & 0 & 0 \\ 0 & w_{ad} & 0 & 0 \\ 0 & 0 & w_{es} & 0 \\ 0 & 0 & 0 & w_{ed} \end{bmatrix} \cdot \begin{bmatrix} 0 & 0 & 1 & 0 \\ 0 & 0 & 0 & 1 \\ 0 & 0 & 0 & 1 \\ 1 & 0 & 0 & 0 \end{bmatrix} \cdot \begin{bmatrix} s \\ d_a \\ d_e \\ d_d \end{bmatrix} \tag{47}
$$

3.2 The MUltiple SIgnal Classification (MUSIC) Algorithm

Subspace methods, such as MUSIC, yield a resolution beyond the limit specified by the

Rayleigh Criterion and therefore are sometimes called "super resolution" methods.

Subspace methods can be used to compute the "pseudo-spectrum" for both the temporal

and spatial signals and both are based on the eigen-decomposition of the correlation

matrix. We will first consider the direction of arrival (DOA) estimation problem.

Consider a linear array illuminated by K-plane waves. We consider these sources to be

uncorrelated. Writing expressions for the signals at the outputs of the antenna elements,

$x_1(t)$, $x_2(t)$, ...,$x_m(t)$. It is possible to express these in a very compact form using the

matrix notation. In order to discern the underlying pattern, it is simpler to start with the

two sources, u_1, u_2 for k = 2 and then generalize to the cave when there are any, say k,

number of sources. Then,

$$x_1(t) = u_1(t)e^{+j\beta d_1 \cos\phi_1} + u_2(t)e^{+j\beta d_1 \cos\phi_2} + n_1(t)$$

$$x_2(t) = u_1(t)e^{+j\beta d_2 \cos\phi_1} + u_2(t)e^{+j\beta d_2 \cos\phi_2} + n_2(t) \qquad (48)$$

$$\vdots \qquad\qquad\qquad \vdots$$

$$x_m(t) = u_1(t)e^{+j\beta d_m \cos\phi_1} + u_2(t)e^{+j\beta d_m \cos\phi_2} + n_m(t)$$

This set of equations may be very compactly expressed as follows:

$$
\begin{bmatrix} x_1(t) \\ x_2(t) \\ \vdots \\ x_m(t) \end{bmatrix}
=
\begin{bmatrix}
e^{+j\beta d_1 \cos\phi_1} & e^{+j\beta d_1 \cos\phi_2} \\
e^{+j\beta d_2 \cos\phi_1} & e^{+j\beta d_2 \cos\phi_2} \\
\vdots & \vdots \\
e^{+j\beta d_m \cos\phi_1} & e^{+j\beta d_m \cos\phi_2}
\end{bmatrix}
\begin{bmatrix} u_1(t) \\ u_2(t) \end{bmatrix}
+
\begin{bmatrix} n_1(t) \\ n_2(t) \\ \vdots \\ n_m(t) \end{bmatrix}
\qquad (49)
$$

Now, we use the following definitions:

$$
\vec{x} = \begin{bmatrix} x_1(t) \\ x_2(t) \\ \vdots \\ x_m(t) \end{bmatrix}
\qquad (50)
$$

$$
\vec{a}(\beta_1) = \begin{bmatrix}
e^{+j\beta d_1 \cos\phi_1} \\
e^{+j\beta d_2 \cos\phi_1} \\
\vdots \\
e^{+j\beta d_m \cos\phi_1}
\end{bmatrix}
\begin{bmatrix} u_1(t) \\ u_2(t) \end{bmatrix}
+
\begin{bmatrix} n_1(t) \\ n_2(t) \\ \vdots \\ n_m(t) \end{bmatrix}
\qquad (51)
$$

$$[\ A\ ] = [\ \vec{a}(\beta_1) \quad \vec{a}(\beta_2)\ ] \qquad (52)$$

$$\beta_1 = \beta\cos\phi_1 \qquad (53)$$

$$\beta_2 = \beta\cos\phi_2 \qquad (54)$$

$$\vec{u} = \begin{bmatrix} u_1 \\ u_2 \end{bmatrix} \tag{55}$$

$$\vec{n} = \begin{bmatrix} n_1 \\ n_2 \\ \vdots \\ n_m \end{bmatrix} \tag{56}$$

Now we can write,

$$\vec{x} = A\,\vec{u} + \vec{n} \tag{57}$$

Here $\vec{x}$ is (Mx1), A is (Mx2), $\vec{u}$ is (2x1) and $\vec{n}$ is (Mx1). To generalize this to any

number of sources, say, k-sources is quite simple. The A matrix is now (M x k) and $\vec{u}$

vector is (R x 1). That is,

$$[\,A\,] = [\;\; \vec{a}(\beta_1) \quad \vec{a}(\beta_2) \quad \ldots \quad \vec{a}(\beta_k) \;\;] \tag{58}$$

and

$$\vec{u} = \begin{bmatrix} u_1 \\ u_2 \\ \ldots \\ u_k \end{bmatrix} \tag{59}$$

Hence, for the general care, the array output vector is given by,

$$\vec{x} = A\,\vec{u} + \vec{n} \tag{60}$$

Incidentally, $\vec{n}$ is the noise vector and we consider noise signals in different array elements to be uncorrelated.

Now let us determine the correlation matrix $R_{\vec{x}}$ corresponding to the vector $\vec{x}$

$$R_{\vec{x}} = E[\ \vec{x}\ \vec{x}^H\ ] \tag{61}$$

$$R_{\vec{x}} = E\left[\ (A\ \vec{u}\ +\ \vec{n}\ )(A\ \vec{u}\ +\ \vec{n})^H\ \right] \tag{62}$$

Since the signals and noise are uncorrelated,

$$E\left[\ A\vec{u}\vec{n}^H\ \right] = 0 \text{ and } E\left[\ \vec{n}(A\ \vec{u})^H\ \right] = 0 \tag{63}$$

$$R_{\vec{x}} = E\left[\ (A\ \vec{u})\ (A\ \vec{u})^H\ \right] + E\left[\ \vec{n}\vec{n}^H\ \right] \tag{64}$$

$$R_{\vec{x}} = E\left[\ A\ \vec{u}\ \vec{u}^H A^H\ \right] + E\left[\ \vec{n}\vec{n}^H\ \right] \tag{65}$$

$$R_{\vec{x}} = A\ R_{\vec{u}}\ A^H\ +\ \sigma^2 I \tag{66}$$

when $R_{\vec{u}} = E[\ \vec{u}\ \vec{u}^H\ ]$ is a k x k matrix and is of rank k. Matrix A, which is an M x k matrix is also of rank K. Since all the sources are uncorrelated. (It is assumed here M>K). Since A and $R_{\vec{u}}$ are of rank K, $AR_{\vec{u}}A$ is also of rank k, even though it is an MxM matrix.

Let us denote $AR_{\vec{u}}A$ by R, which is MxM but has a rank of K (<M) and we have shown

$$R\vec{x} = \bar{R}\ +\ \sigma^2 I$$

Since $\bar{R}$ is only of rank K, it has K non-zero eigen values $\mu_1 > \mu_2 ...> \mu_k$ and (M-k) zero eigenvalues. Let the eigonvectors of $\bar{R}$ be designated by $\vec{q}_i$, i = 1, 2 ... m. Then,

$$\bar{R}\vec{q}_i = \mu_i\vec{q}_i \quad i = 1, 2 \ldots m \quad \text{and} \quad \mu_i = 0 \quad i = k+1, k+2 \ldots m$$

Now, let us consider $R_{\vec{x}}\vec{q}_i$:

$$R_{\vec{x}}\vec{q}_i = (\bar{R} + \sigma^2 I)\vec{q}_i \tag{67}$$

Therefore, $\vec{q}_i$, the eigenvectors of $\bar{R}$ are also the eigenvectors of $R\vec{x}$ and the eigenvalues

of $R\vec{x}$ are $\lambda_1 > \lambda_2 \ldots > \lambda_m$ and are given by

$$\lambda_i = \mu_i + \sigma^2 \tag{68}$$

Thus, the lowest (M-k) eigenvalues all have the same value of σ^2. That is, $\lambda_i = \sigma^2$ i =

k+1, k+2...M.   Let us now consider the eigendecomposition of $R\vec{x}$.

$$R\vec{x} = \sum_{i=1}^{M} \lambda_i \vec{q}_i \vec{q}_i^H = Q\Lambda Q^H \tag{69}$$

where $Q = \begin{bmatrix} \vec{q}_1 & \vec{q}_2 & \ldots & \vec{q}_m \end{bmatrix}$ and $\Lambda = \text{diag}[\begin{array}{cccc} \lambda_1 & \lambda_2 & \ldots & \lambda_m \end{array}]$

Now, for any i>k, we have

$$R_{\vec{x}}\vec{q}_i = \lambda_i\vec{q}_i = \sigma^2\vec{q}_i \quad \text{for i=K+1,K+2...M}$$

However, since $R_{\vec{x}} = (AR_uA^H + \sigma^2 I)$

$$R_{\vec{x}}\vec{q}_i = (AR_uA^H + \sigma^2 I)\vec{q}_i \tag{70}$$

$$R_{\vec{x}}\vec{q}_i = AR_uA^H\vec{q}_i + \sigma^2\vec{q}_i = \sigma^2\vec{q}_i \tag{71}$$

$$AR_uA^H\vec{q}_i = 0 \tag{72}$$

26

Since AR_u is an M x k matrix of full rank, we get

$$A^H \vec{q}_i = 0 \qquad (73)$$

or stated differently

$$\begin{bmatrix} \vec{a}^H(\beta_1) \\ \vec{a}^H(\beta_2) \\ \vdots \\ \vec{a}^H(\beta_m) \end{bmatrix} \vec{q}_i = 0 \qquad (74)$$

$$\vec{a}^H(\beta_l) \, \vec{q}_i = 0 \text{ for any } l=1,2..k \text{ and } i=k+1,k+2...M$$

This remarkable result states simply that the direction vectors, or "steering vectors,"

$\vec{a}^H(\beta_l)$ for any corresponding to actual direction of arrival are orthogonal to the

eigenvectors associated with the lowest, repeating eigenvalues of the correlation matrix.

The (M-k) dimensional subspace spanned by the eigenvectors $\begin{bmatrix} \vec{q}_{k+1} & \vec{q}_{k+2} & \cdots & \vec{q}_m \end{bmatrix}$

is called the noise subspace N and every direction vector associated with the true arrival

angle is orthogonal to the entire subspace. This noise subspace N is orthogonal to the k

dimensional subspace spanned by $\begin{bmatrix} \vec{q}_1 & \vec{q}_2 & \cdots & \vec{q}_k \end{bmatrix}$ which is designated by S and is

called the signal subspace.

We use these remarkable properties to determine the direction of arrival. Let us define

the "direction vector" or the "search vector"

$$\vec{a}(\beta_1) = [\; e^{+j\beta d_1 \cos\phi_1} \quad e^{+j\beta d_2 \cos\phi_1} \quad : \quad e^{+j\beta d_m \cos\phi_1} \;]^T$$

Where, the MUSIC pseudo-spectrum is given by:

$$\hat{P}(\beta)_{MUSIC} = \frac{1}{\displaystyle\sum_{i=k+1}^{N} \left| \vec{q}_i^{\,H} \vec{a}(\beta) \right|^2} \tag{75}$$

When β corresponds to the true direction of arrival, then the denominator approaches zero resulting in a sharp peak of the function $P(\beta)$. Note that the peaks occur irrespective of the separation between the actual angles of arrival. Thus, this estimator, in principle, can resolve arbitrarily close targets.

3.3 AMP MUSIC System Model

By combining the Adaptive Monopulse (AMP) technique and MUltiple SIgnal Classification (MUSIC) Algorithm, angle estimation in a mainbeam jamming environment can be accomplished. The pseudo-spectrum (**P Surface**) is defined as:

$$P(\alpha,\varepsilon) = \frac{1}{\displaystyle\sum_{i=k+1}^{N} \left| \vec{q}_i^{\,H} \vec{a}(\alpha,\varepsilon) \right|^2} \tag{76}$$

where,

$\vec{q} \equiv$ eigenvector $\qquad\qquad \vec{a}(\alpha,\varepsilon) \equiv$ direction vector
$\lambda \equiv$ eigenvalue $\qquad\qquad\quad P(\alpha,\varepsilon) \equiv$ MUSIC Spectrum
$R = Q\Lambda Q^H \equiv$ Covariance
$\vec{q}_i^{\,H} \vec{a}\,(\beta_l) = 0$ for any $l = 1,2,\ldots, k$, and $i = k+1, k+2,\ldots, N$

Since each of these signals is orthogonal to the noise subspace, the denominator goes to zero when:

$$\vec{q}_i^{\,H} \vec{a}\,(\beta_l) = 0 \tag{77}$$

for any $l = 1,2,\ldots, k$, and $i = k+1, k+2,\ldots, N$

$$\beta_l = \alpha_l, \varepsilon_l \tag{78}$$

For a monopulse system $N = 4$ and k = the size of the noise space. Giving the following

equations:

$$\beta_x = \sin(\alpha)\cos(\varepsilon) \tag{79}$$

$$\beta_y = \sin(\varepsilon) \tag{80}$$

$$\vec{a}(\alpha,\varepsilon) = \begin{bmatrix} e^{j\beta_x x1} e^{j\beta_y y1} \\ e^{j\beta_x x2} e^{j\beta_y y2} \\ e^{j\beta_x x3} e^{j\beta_y y3} \\ e^{j\beta_x x4} e^{j\beta_y y4} \end{bmatrix} \tag{81}$$

The monopulse P Surface is defined as:

$$P(\alpha,\varepsilon) = \frac{1}{\displaystyle\sum_{i=k+1}^{4} \left| \vec{q}_i^{H} M\vec{a}(\alpha,\varepsilon) \right|^2} \tag{82}$$

where M is the monopulse transformation matrix. The AMP MUSIC system model is
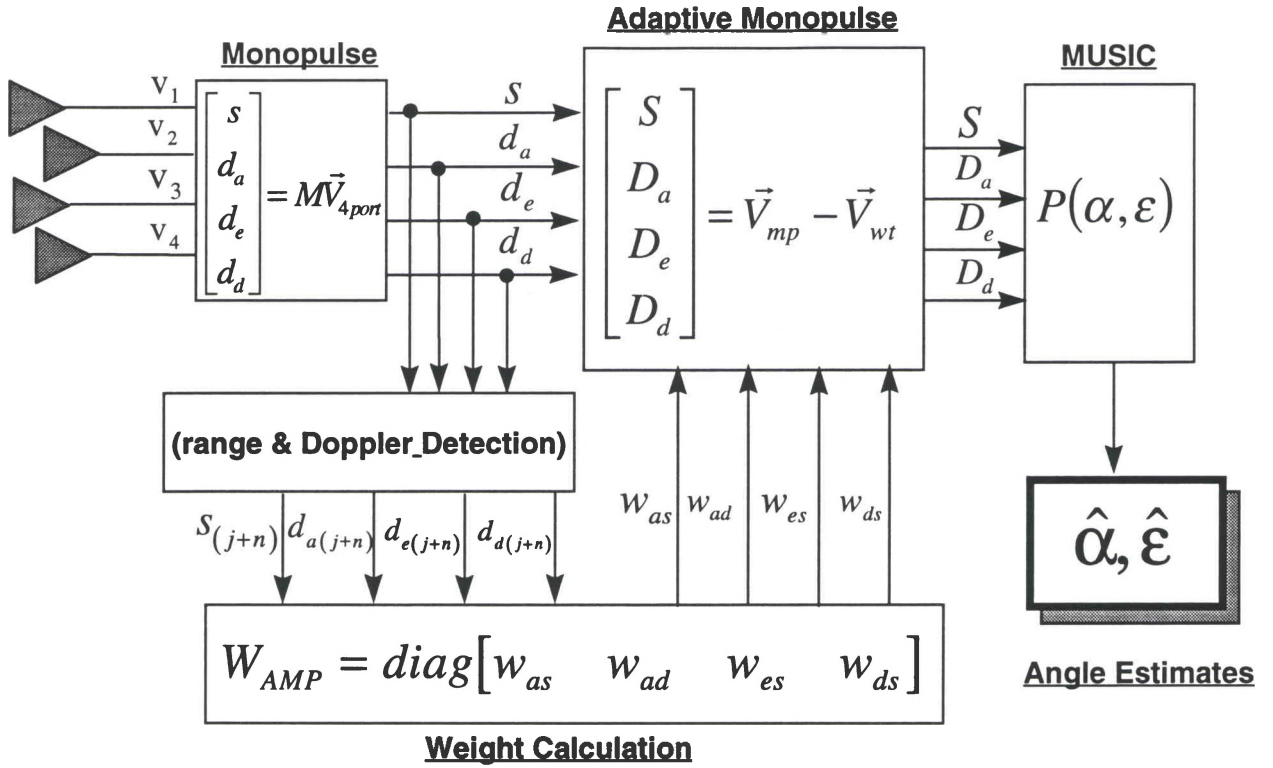
shown in figure 13 below.

Figure 13. System.

The number of jammers is determined through correlation and eigenvalue analysis. The size of the noise space k is determined by examining the relative size of the eigenvalues. Noise space eigenvalues will be considerably lower in magnitude than signal space eigenvalues as shown in figure 14.
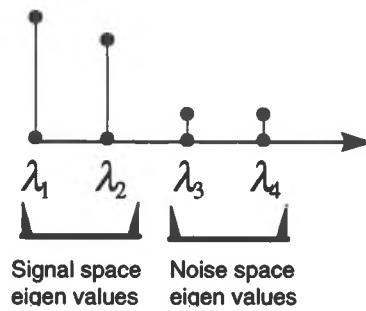

Figure 14. Signal and Noise Values.

The noise subspace eigenvectors $\vec{q}_i$ corresponding to the noise subspace eigenvalues λ_i (recall that $\vec{q}_i \Leftrightarrow \lambda_i$) are used in the P surface equation. They are calculated from the correlation matrix $R_{\vec{V}_{AMP}}$, which is, calculated from $\vec{V}_{AMP}$ which is the voltage output of the adaptive monopulse system.

$$\vec{q} \equiv \text{eigenvector} \qquad\qquad \lambda \equiv \text{eigenvalue}$$

The eigenvector matrix Q and eigenvalue matrix L are both reordered by eigenvalue magnitude as in figure 14 and the noise subspace is used to calculate P.

$$R_{\vec{V}_{AMP}} = E[\ \vec{V}_{AMP}\ \vec{V}_{AMP}^H] \tag{83}$$

$$Q = [\ \vec{q}_1\ \vec{q}_2\ \vec{q}_3\ \vec{q}_4\ ] \tag{84}$$

$$\vec{V}_{AMP} = \begin{bmatrix} S \\ D_a \\ D_e \\ D_d \end{bmatrix} \qquad\qquad \Lambda = \begin{bmatrix} \lambda_1 & 0 & 0 & 0 \\ 0 & \lambda_2 & 0 & 0 \\ 0 & 0 & \lambda_3 & 0 \\ 0 & 0 & 0 & \lambda_4 \end{bmatrix} \tag{85}$$

The AMP MUSIC method involves projection of the signal onto the entire noise subspace to calculate P. However, the AMP MUSIC Pseudo-spectrum (P Surface) only provides us with signal location and does not indicate which peak corresponds to the target and which peak corresponds to the nulled jammer.
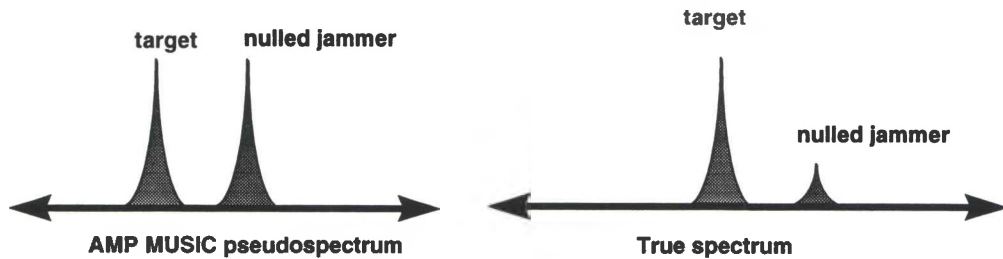

Figure 15. AMP MUSIC Spectrum.

3.4 Signal Power Estimation

The true powers corresponding to the two peaks in the pseudo spectrum are computed using the least square estimation of signal amplitudes. The signal with the highest power is declared to be the target signal. The rationale for such a decision is that the jammer signal is severely attenuated by the adaptation process leaving the target signal to be the dominant component. The peak locations of the pseudo spectrum yield two angle estimates leading to two steering vectors, $u_1(t_k)$ and $u_2(t_k)$ which can be used to define this following signal model at time instant t_k :

$$\vec{V}(t_k)_{AMP} = \begin{bmatrix} S(t_k) \\ D_a(t_k) \\ D_e(t_k) \\ D_d(t_k) \end{bmatrix} = [\, \vec{MA_1} \,\, \vec{MA_2} \,] \cdot \begin{bmatrix} u_1(t_k) \\ u_2(t_k) \end{bmatrix} + \varepsilon \tag{86}$$

Here ε is the modeling error. $[\, \vec{MA_1} \,\, \vec{MA_2} \,]$ are the unknowns. Note that the frequencies of operation, ω_1 and ω_2 may be unknown and are clubbed together with the phases ψ_1 and ψ_2.

$$\begin{bmatrix} u_1(t_k) \\ u_2(t_k) \end{bmatrix} = \begin{bmatrix} A_1 e^{j\psi_x} e^{j\omega_1 t_k} \\ A_2 e^{j\psi_x} e^{j\omega_2 t_k} \end{bmatrix} = [(M'(M')^H]^{-1} (M')^H \, \vec{V}(t_k)_{AMP}$$

$$M' = [\, \vec{MA_1} \,\, \vec{MA_2} \,] \tag{87}$$

After determining which peaks corresponds to target and jammer, the jammer peak can be ignored or removed and angle estimation can be made.

CHAPTER 4

RESULTS

The theory presented earlier is used to develop an extensive simulation running under

MATLAB environment. This simulation is used to evaluate the statistical properties of

the newly developed estimator. The procedures used in the analysis presented in this

chapter were set fort in [6] and [17]. Baseline sets of simulations have been carried out to

record the performance of the estimator in the absence of jamming. In addition an

extensive sequence of simulations are carried out to examine the following issues:

i)   Effect of SNR

ii)   Effect of covariance matrix estimation losses.

iii)   Effect of JNR

iv)   Effect of the proximity of jammer.

The statistics of the estimates shown in this thesis are based mostly on 100 trials.

We examine the ideal case of no jamming first. Figure 16 shows a typical plot of $\mathbf{P}(\alpha,\varepsilon)$

over the range $-100^{\circ} < \alpha,\varepsilon < 100^{\circ}$ for $\alpha_d = \varepsilon_d = 0^{\circ}$, SNR = 10 dB, $\psi_d = 0^{\circ}$ and $l = \dfrac{\lambda}{2}$. As

may be seen, $\mathbf{P}(\alpha,\varepsilon)$ is a smooth flat surface with a single sharp peak at the desired signal

angles. Figure 17 shows a contour plot of this surface. Figure 18 shows another example

of $P(\alpha,\varepsilon)$ with no jamming, for $\alpha_d = \varepsilon_d = 20°$ (and SNR = 10 dB, $\psi_d = 0°$). The corresponding contour plot is shown in Figure 19. Note that the peak broadens in width but is accurate in angle estimate.

The peak of $P(\alpha,\varepsilon)$ always occurs at $(\alpha_d, \varepsilon_d)$. By finding the peak of $P(\alpha,\varepsilon)$ for each, we can plot the estimated angles as functions of the actual angles.

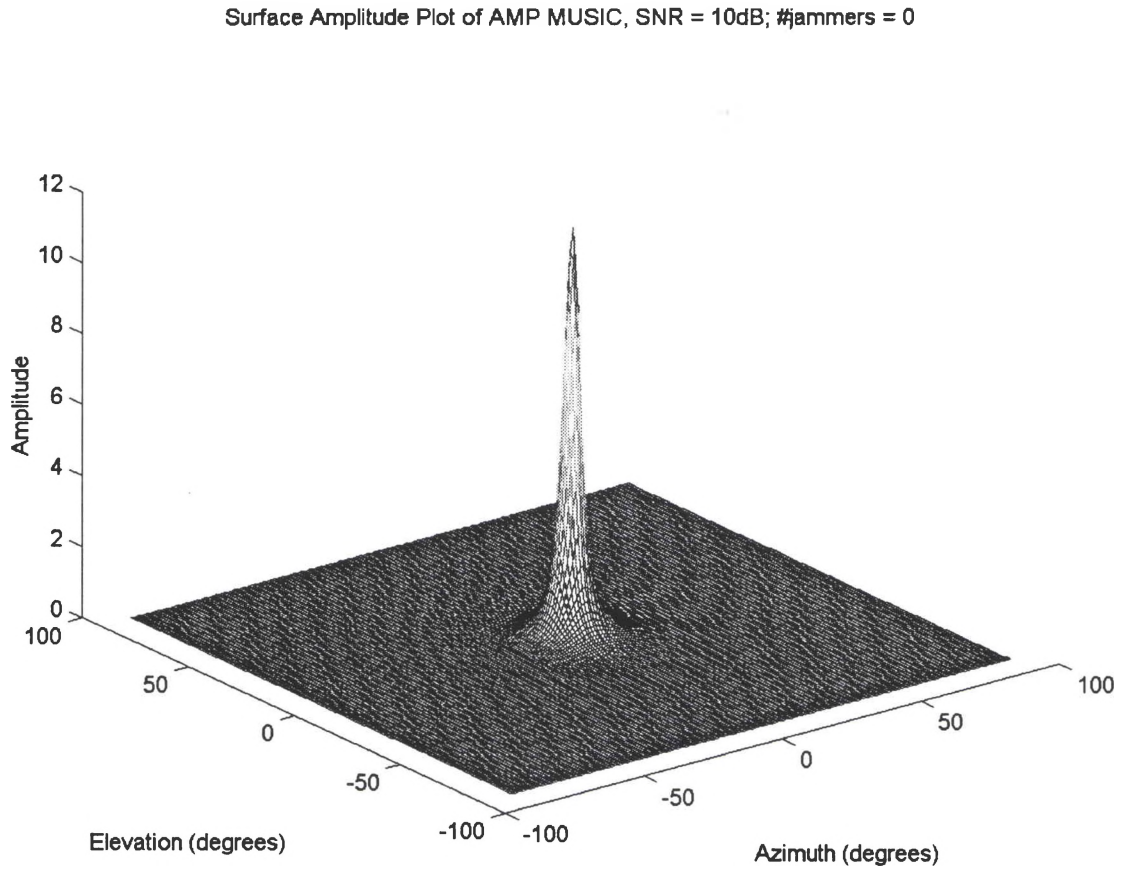Surface Amplitude Plot of AMP MUSIC, SNR = 10dB; #jammers = 0

Figure 16. AMP MUSIC Spectrum for $\alpha d = \varepsilon d = 0$, no jamming and L = 8.
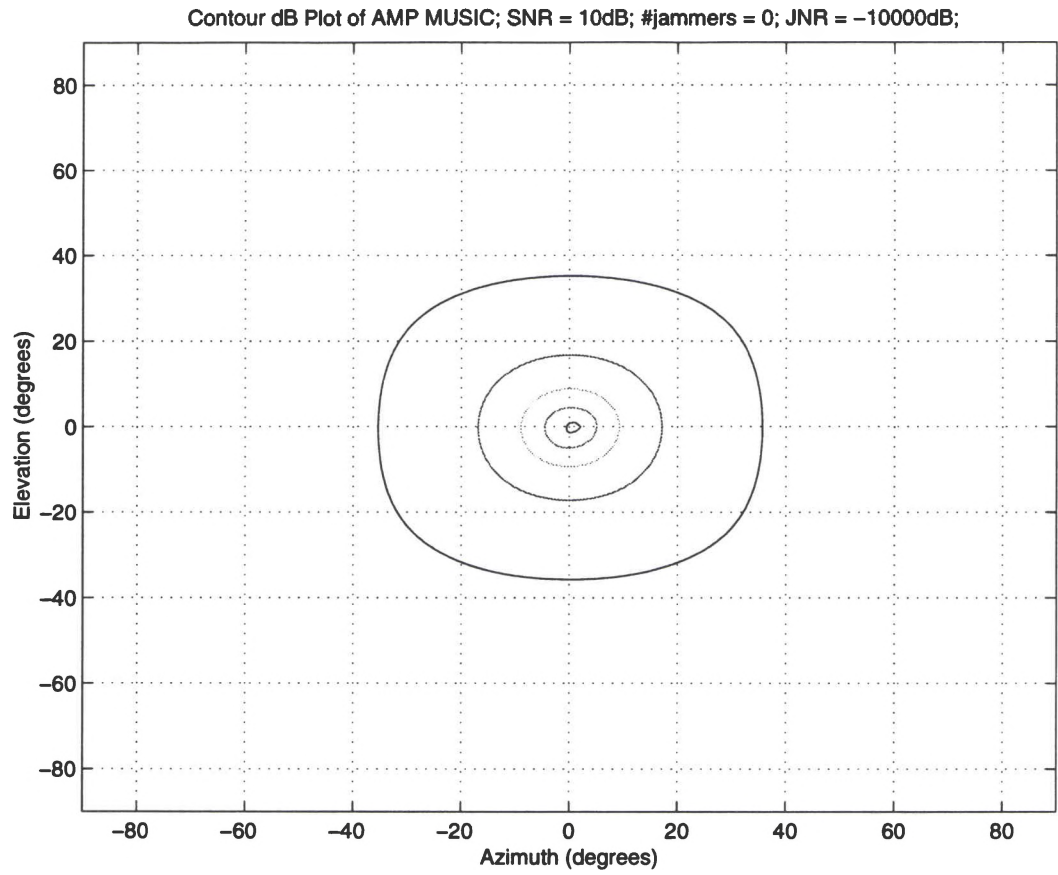
Figure 17. Contours of constant Px in α,ε-plane for $\alpha d = \varepsilon d = 0$, no jamming and L = 8.

Surface Amplitude Plot of AMP MUSIC, SNR = 10dB; #jammers = 0

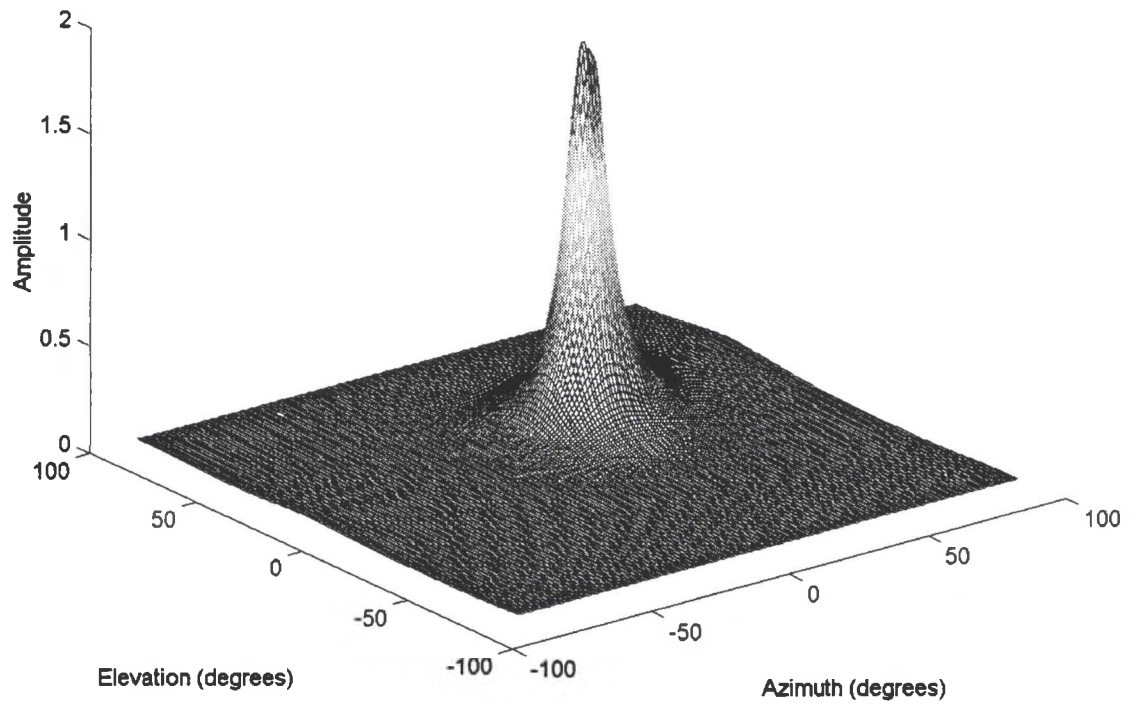**Figure 18.** AMP MUSIC Spectrum for $\alpha d = \varepsilon d = 20$, no jamming and L = 8.
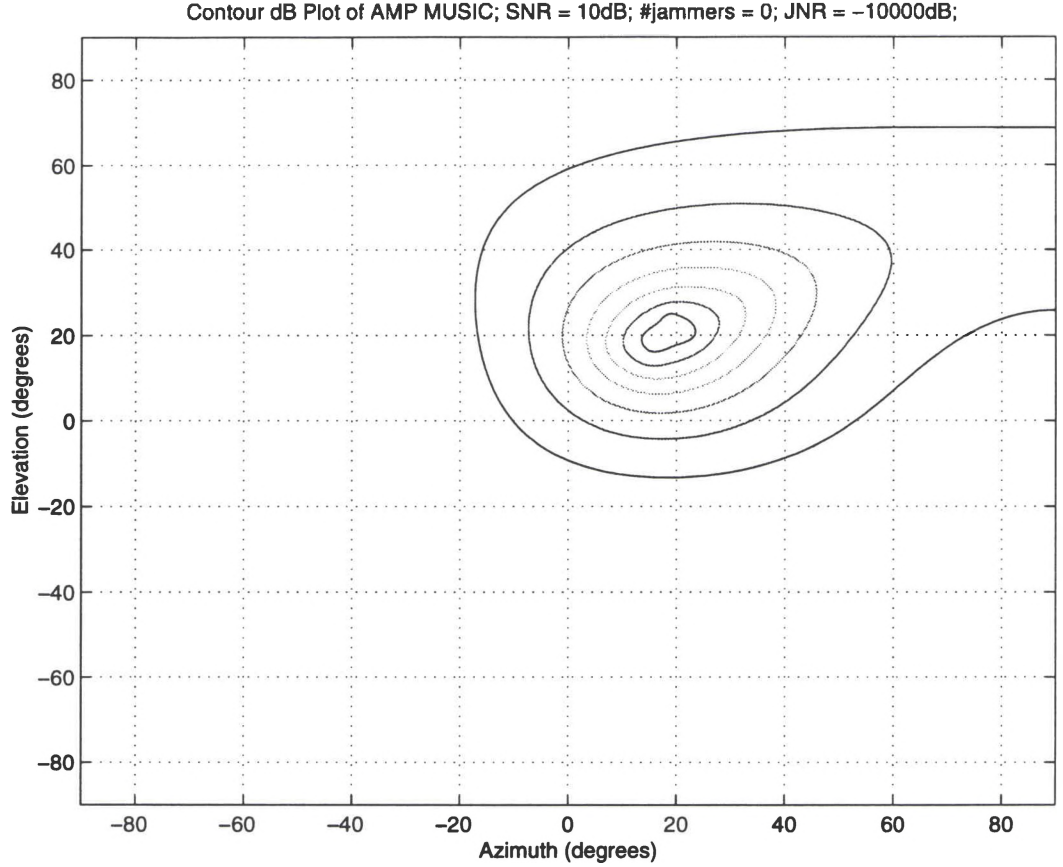
Figure 19. Contours of constant Px in α,ε-plane for $\alpha d = \varepsilon d = 20$, no jamming and $L = 8$.

Now we examine some Monte Carlo run examples. First, Figure 20 shows a typical set of azimuth estimates obtained in 100 Monte Carlo trials when the SNR is $\xi_d = 10$ dB, the signal arrives $\alpha_d = \varepsilon_d = 1^o$, there is no jamming, and $L = 8$ signal vectors are used in the covariance matrix. Note that this SNR is low. As may be seen, the estimates are right on $\alpha_d = 1^o$ with occasional estimates having large error. The reason for these bad estimates is that the search routine used to locate the peak of $P(\alpha,\varepsilon)$ found a local maximum, due to noise, instead of the global maximum. Since AMP MUSIC estimation requires a search to find the peak of $P(\alpha,\varepsilon)$, this problem can sometimes occur. Naturally, when the search

37

finds the wrong peak, the error is very large. This problem is rare at high SNR as shown in Figure 21. Figure 21 shows a set of 100 estimates obtained when the SNR = 10 dB and the other parameters are the same as in Figure 20. A SNR of 10 dB is considered low but shown here to demonstrate performance increase.

Given a set of N estimates such as those in Figure 20, we define the sample average of the set to be

$$Av(\alpha_d) = \frac{1}{N} \sum_{n=1}^{N} \alpha_d(n) \tag{88}$$

where $\alpha_d(n)$ denotes the nth estimate in the set. The sample bias of the set is then

$$Av(\alpha_d) - \alpha_d$$

and the sample standard deviation is

$$\frac{1}{N-1} \{ \sum_{n=1}^{N} [\alpha_d - Av(\alpha_d)] \} \tag{89}$$

If the SNR is reduced, the estimates become noisier. Note that some of the estimates in Figure 21 still have very large error. When the SNR is too low, the estimates no longer have much relationship to the actual angle.
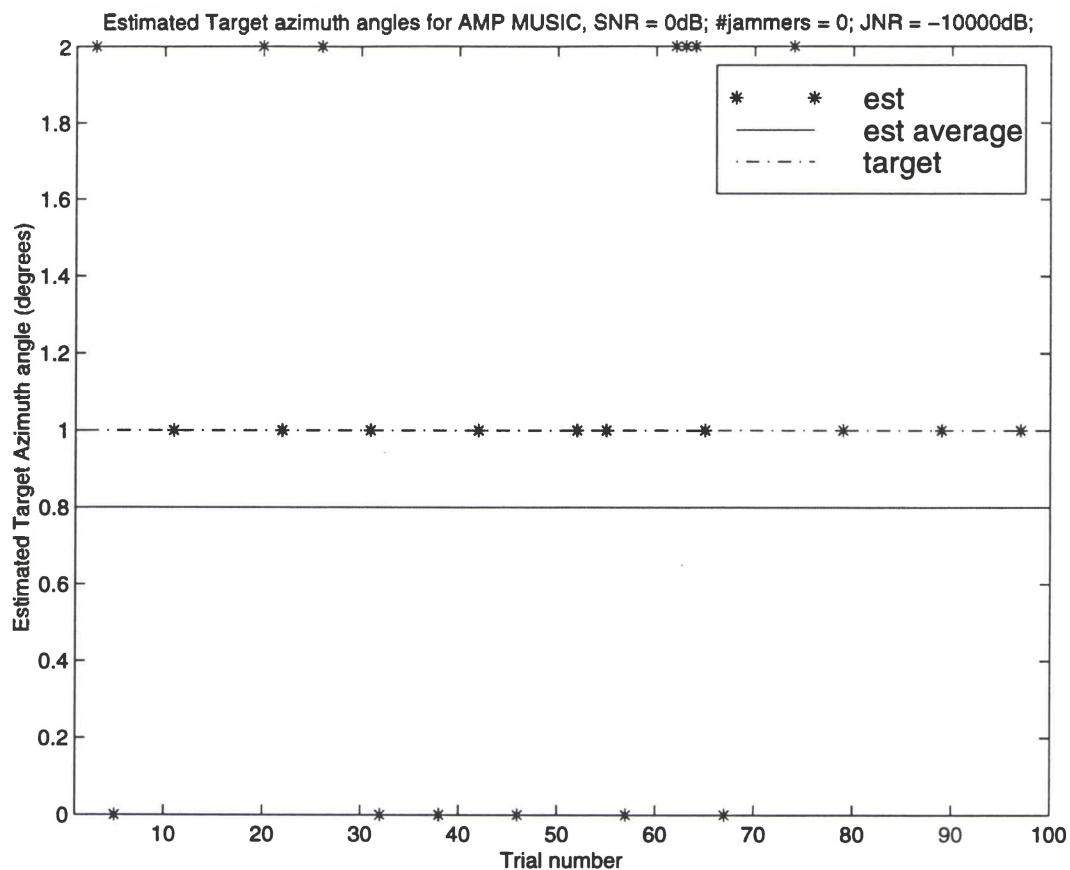
Figure 20. Estimated azimuth angles for 100 Monte Carlo trials with ξd = 0 dB, αd = εd = 1, no jamming and L = 8.
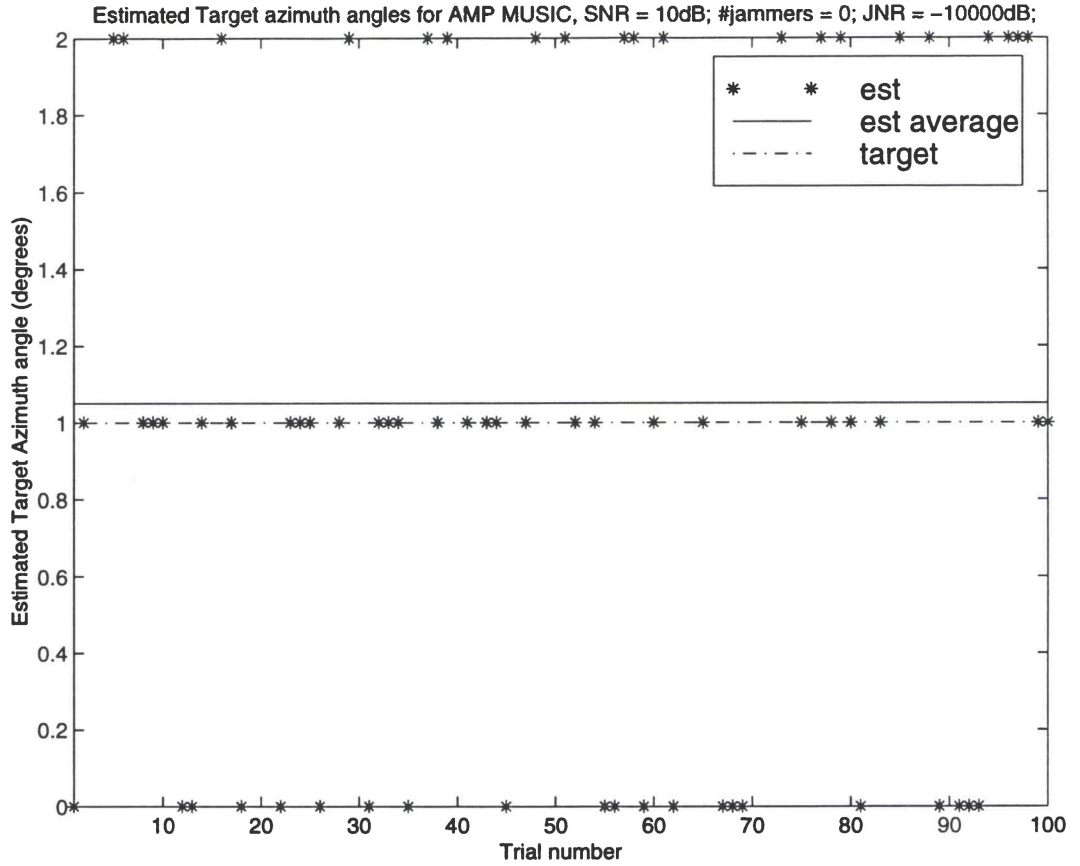
Figure 21. Estimated azimuth angles for 100 Monte Carlo trials with $\xi_d = 10$ dB, $\alpha_d = \varepsilon_d = 1$, no jamming and L = 8.

4.1 The Effect of SNR

How the desired signal SNR (ξ_{5d}) affects the performance of the estimates is shown in

Figures 22-25. Figure 22 shows the azimuth bias (the average error in α_d) vs. the desired

signal SNR when the desired signal arrives from $\alpha_d = \varepsilon_d = 1^o$ and there is no jamming.

Figure 23 shows the standard deviation of α_d, and Figures 24 and 25 show the bias and

standard deviation of the elevation estimate ε_d all as functions of the SNR. The curves in

Figures 22-25 were obtained by averaging the results of 100 independent trials for each SNR. For each trial, the covariance matrix was computed from $L = 8$ signal vectors. Because the biases and standard deviations shown in Figures 22-25 are computed from a finite number of trials, they are themselves estimates of the true biases and standard deviations. In general, the more trials used to form the estimates, the less the variance of these estimates. To see how the number of trials affects these curves, Figures 26-29 show the biases and standard deviations of α_d and ε_d obtained when 400 trials are averaged and $L = 24$. Note that the curves are much smoother in this case. Most of the results in this thesis have been obtained by averaging 100 Monte Carlo trials. We note from Figures 22-25 (or 26-29) that the bias and standard deviation of ε_d are essentially the same as those for α_d. As expected high SNR yields low to zero bias and standard deviation.
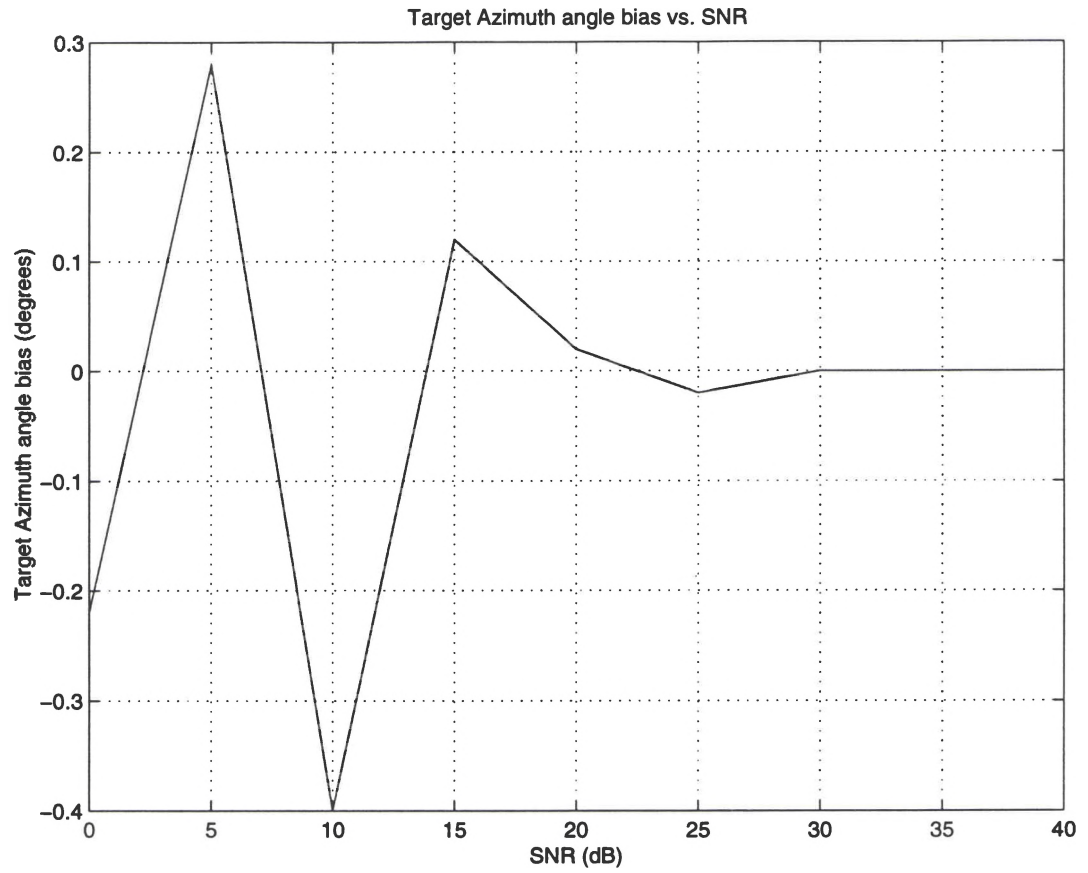
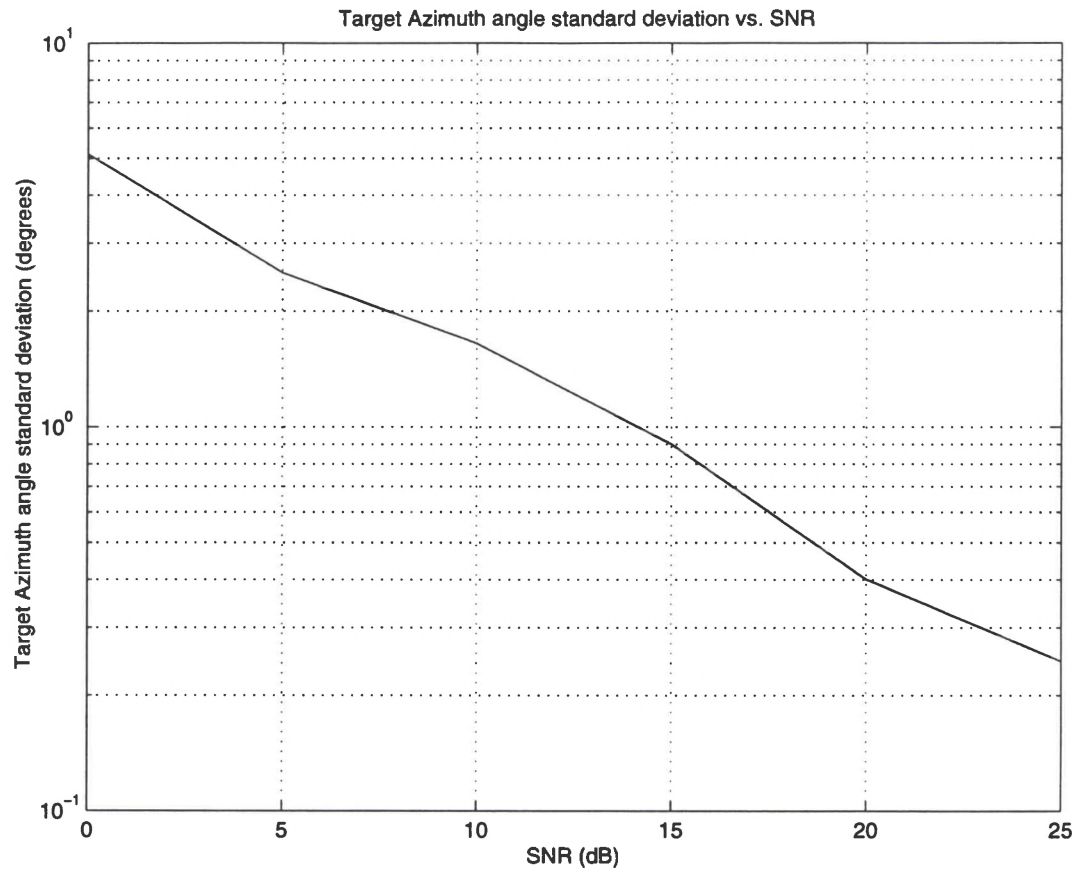**Figure 22.** Azimuth bias vs. SNR for $\alpha = \varepsilon = 1$, no jamming and $L = 8$. Curve is computed from 100 trials.

Figure 23. Azimuth standard deviation vs. SNR for $\alpha d = \varepsilon d = 1$, no jamming and $L = 8$. Curve is computed from 100 trials.
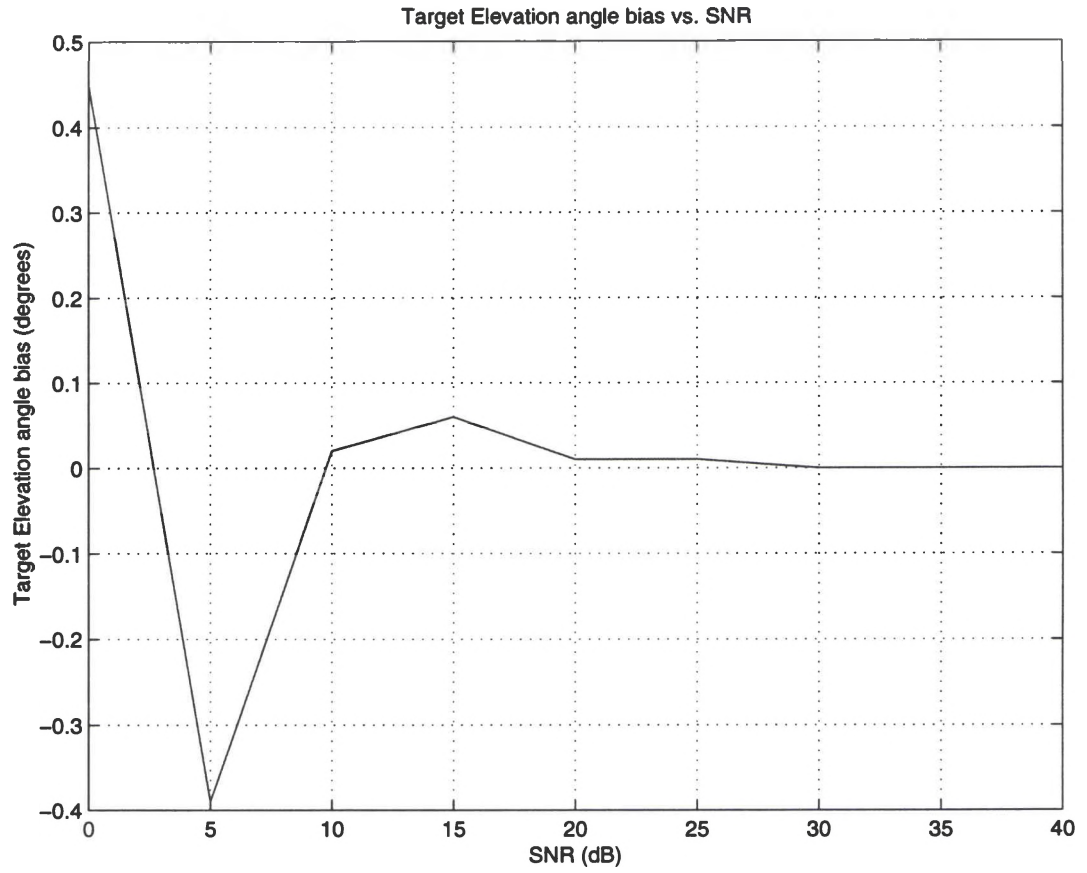
Figure 24. Elevation bias vs. SNR for $\alpha d = \epsilon d = 1$, no jamming and L = 8. Curve is computed from 100 trials.
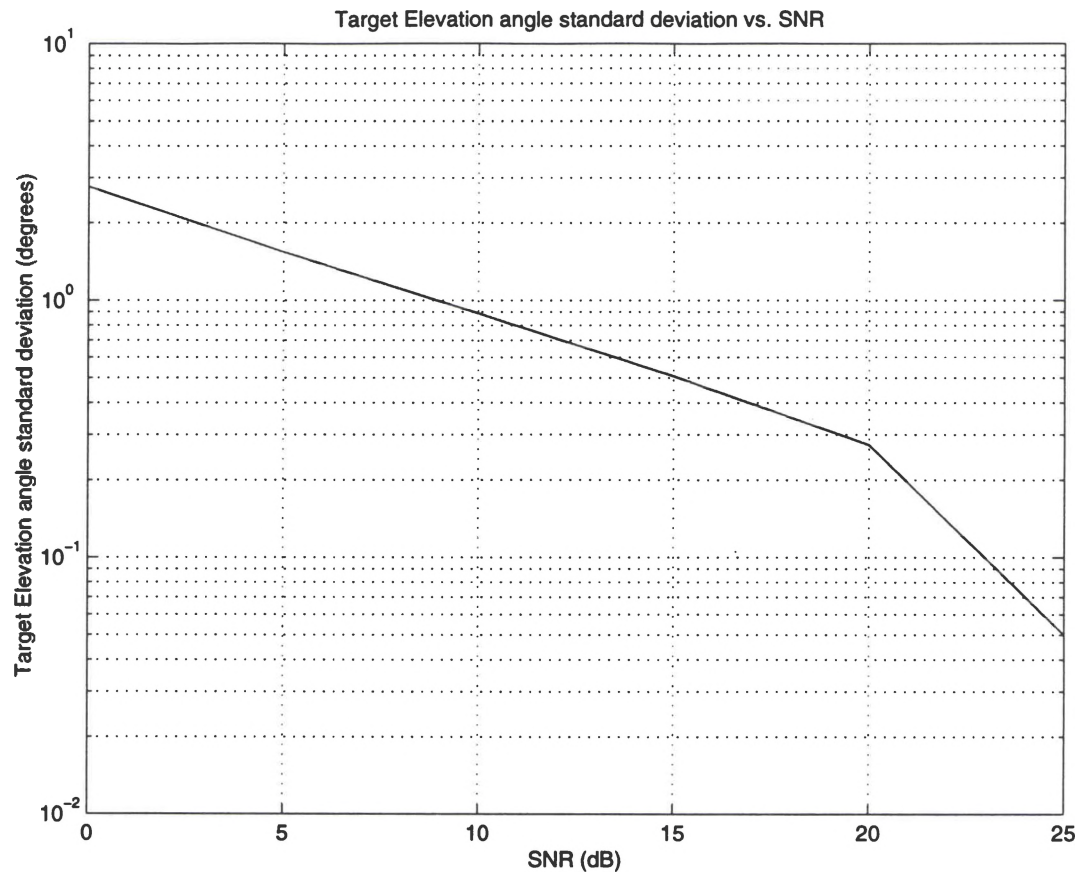
Figure 25. Elevation standard deviation vs. SNR for $\alpha d = \varepsilon d = 1$, no jamming and L = 8. Curve is computed from 100 trials.
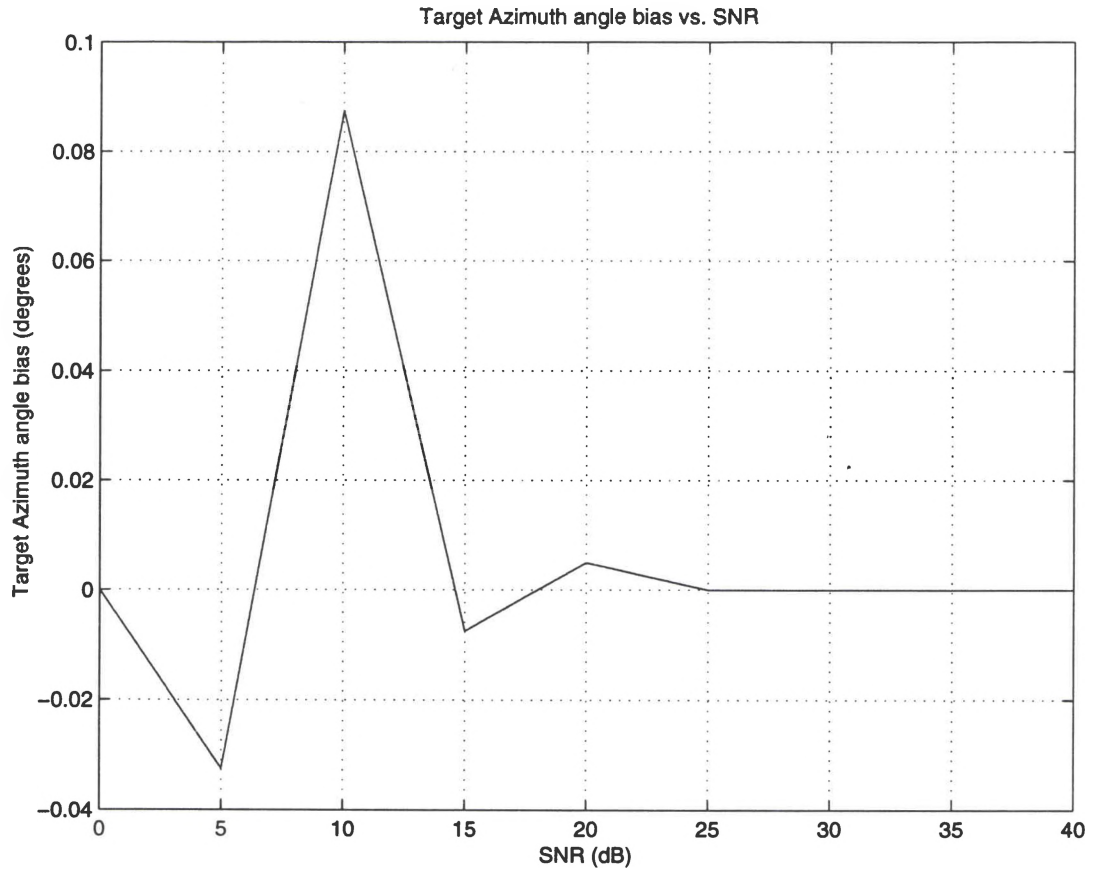
Figure 26. Azimuth bias vs. SNR for $\alpha d = \varepsilon d = 1$, no jamming and L = 24. Curve is computed from 400 trials.
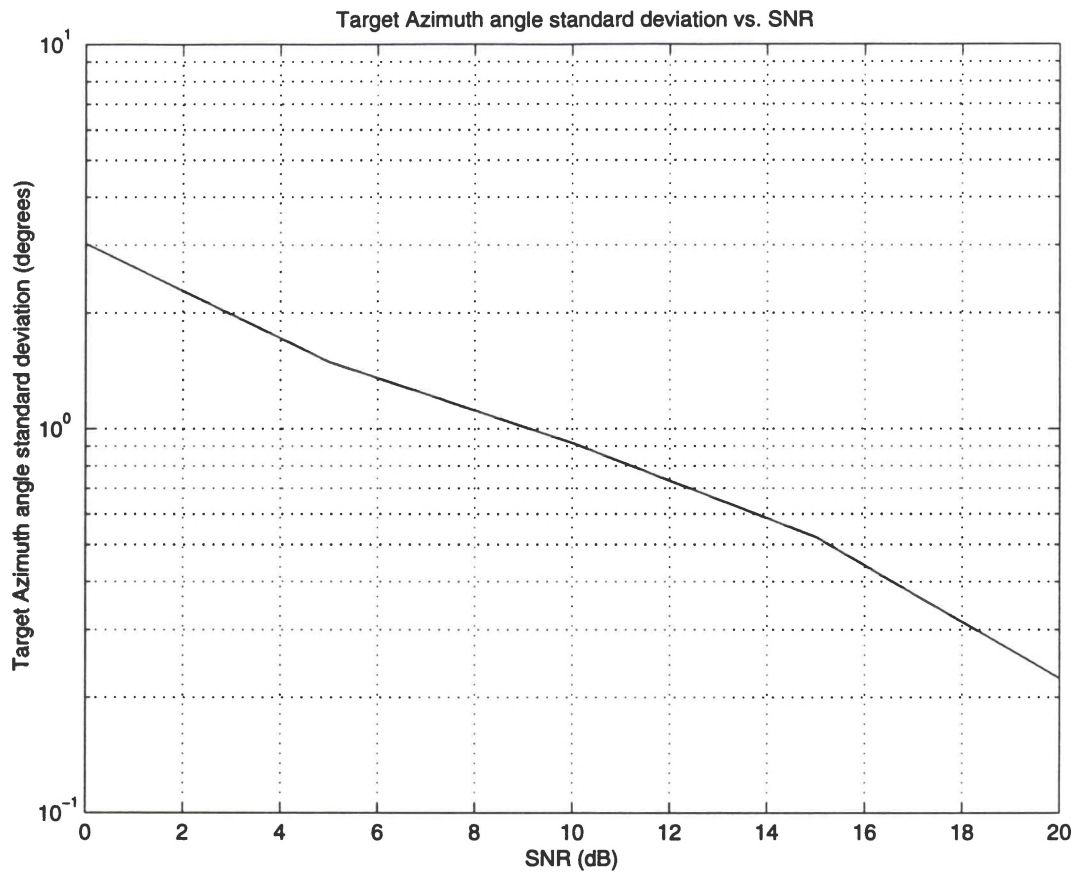
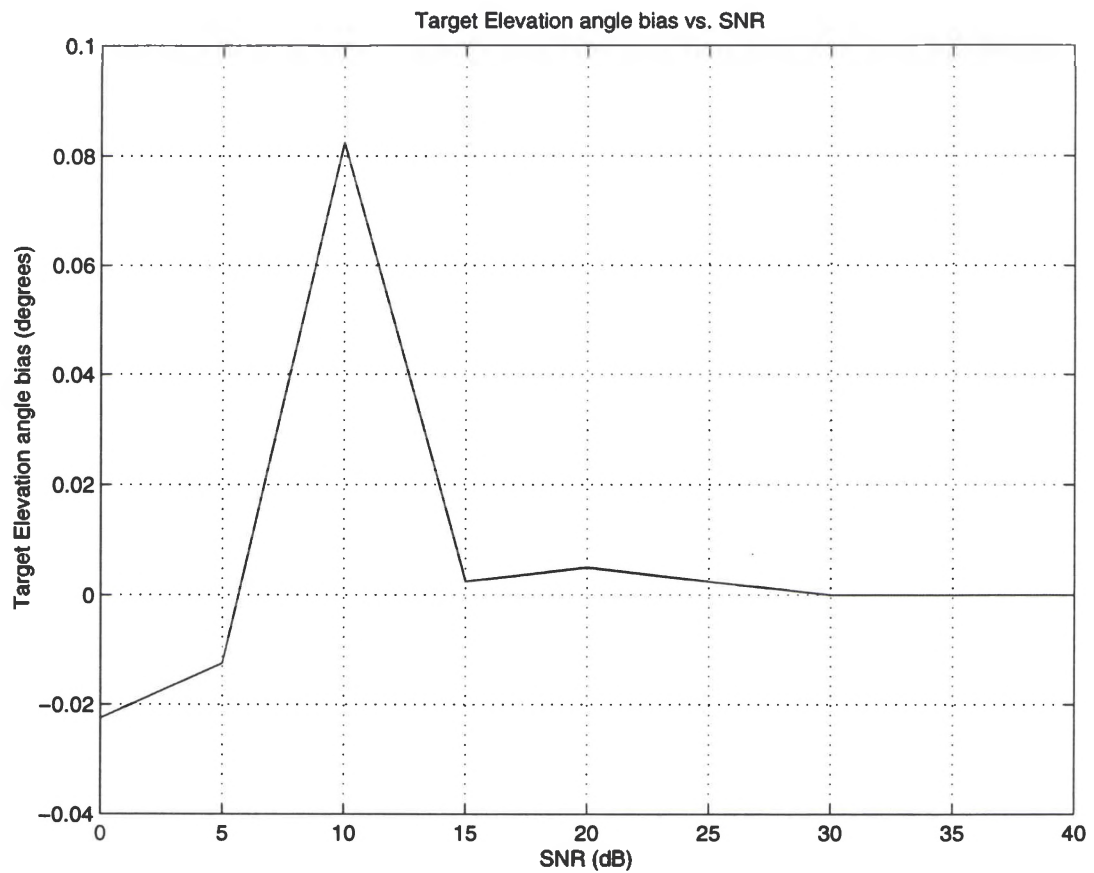**Figure 27.** Azimuth standard deviation vs. SNR for αd = εd = 1, no jamming and L = 24. Curve is computed from 400 trials.

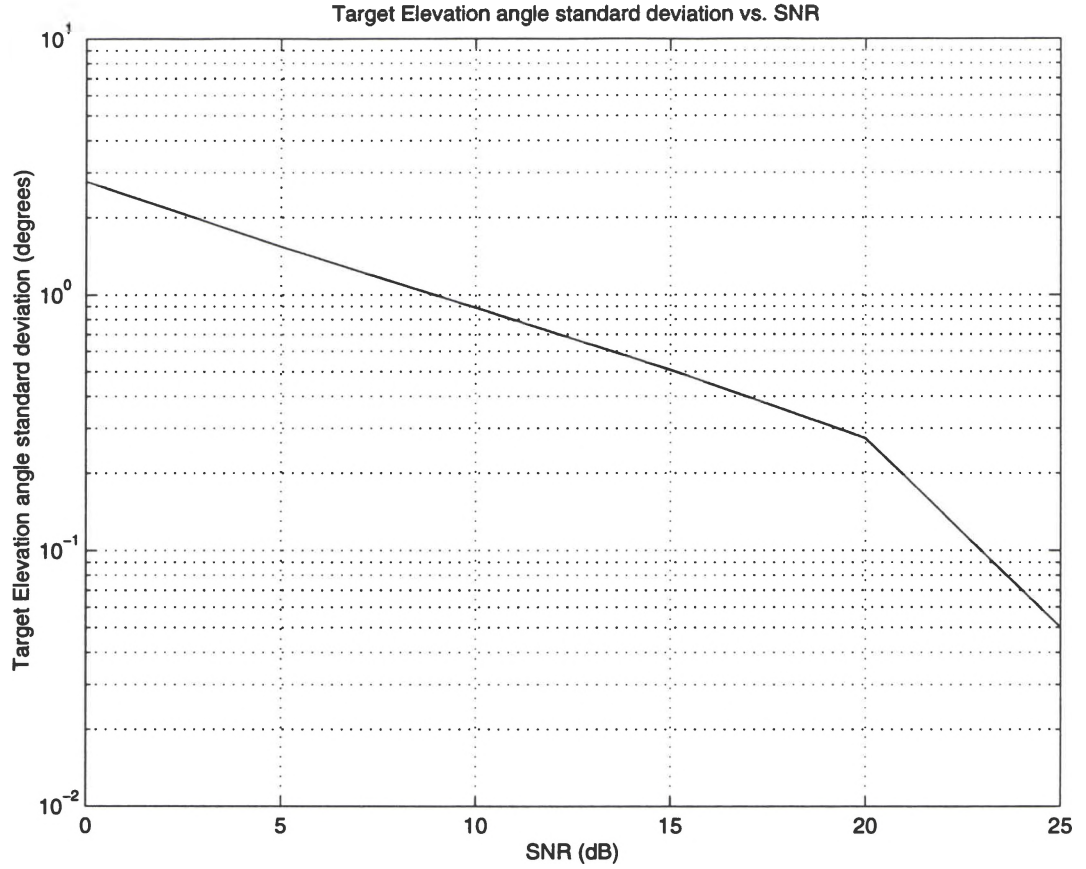**Figure 28.** Elevation bias vs. SNR for αd = εd = 1, no jamming and L = 24. Curve is computed from 400 trials.

Figure 29. Elevation standard deviation vs. SNR for $\alpha d = \varepsilon d = 1$, no jamming and $L = 24$. Curve is computed from 400 trials.

4.2 The Effect of L

Now we look at how the bias and standard deviation of α_d and ε_d are affected by a number of signal vectors L used to form the covariance matrix. The curves in Figures 30-33 are computed for an SNR of $\xi_d = 30$ dB, $\alpha_d = \varepsilon_d = 1^{\circ}$ and no jamming. Note that since the covariance matrix is a 4 x 4 matrix, L must be at least 4 to make M nonsingular. In Figures 30-33, the means and variances of α_d and ε_d are shown for $1 < L < 20$. These curves show that the standard deviations of α_d and ε_d do not improve for L larger than

49

about 5 or 6. Reed, Mallett and Brennan [18] stated that L should be twice the number of adaptive channels, or in this case 8. For most curves in this thesis, we have used L=8. However, it is interesting to see what happens if more trials are used to compute the bias and standard deviation. Figures 34 and 35 show the standard deviations of α_d and ε_d computed from 400 Monte Carlo trials. These curves show that the standard deviation becomes negligible at about $L = 6$ not necessarily $L = 5$. The explanation for this difference appears to be that with 100 trials, the variance in the computed standard deviation is large enough to mask any improvement for L>5. However, with 400 trials, the variance in the computed standard deviation is smaller so the improvement for L>5 can be seen.

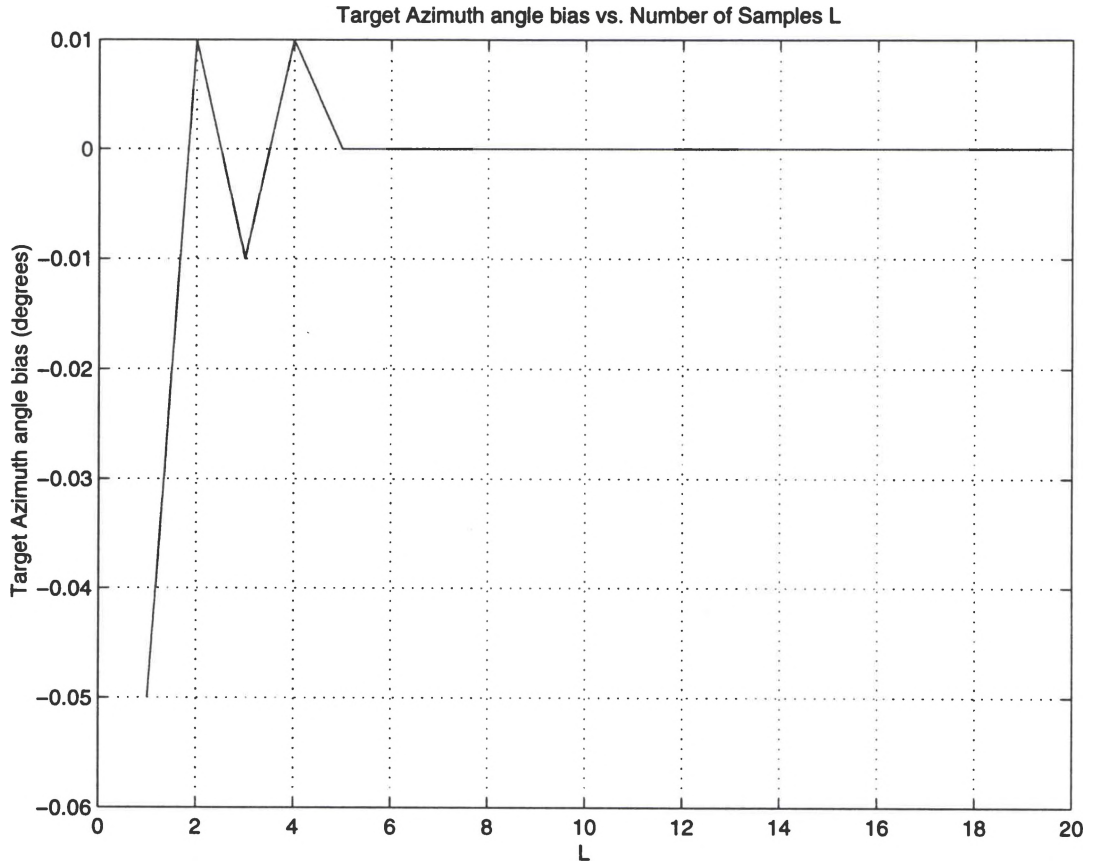Target Azimuth angle bias vs. Number of Samples L

Figure 30. Azimuth bias vs. L for ξd = 30 dB, αd = εd = 1, and no jamming. Curve is computed from 100 trials.

Figure 31. Azimuth standard deviation vs. L for ξd = 30 dB, αd = εd = 1, and no jamming. Curve is computed from 100 trials.

Figure 32. Elevation bias vs. L for ξd = 30 dB, αd = εd = 1, and no jamming. Curve is computed from 100 trials.

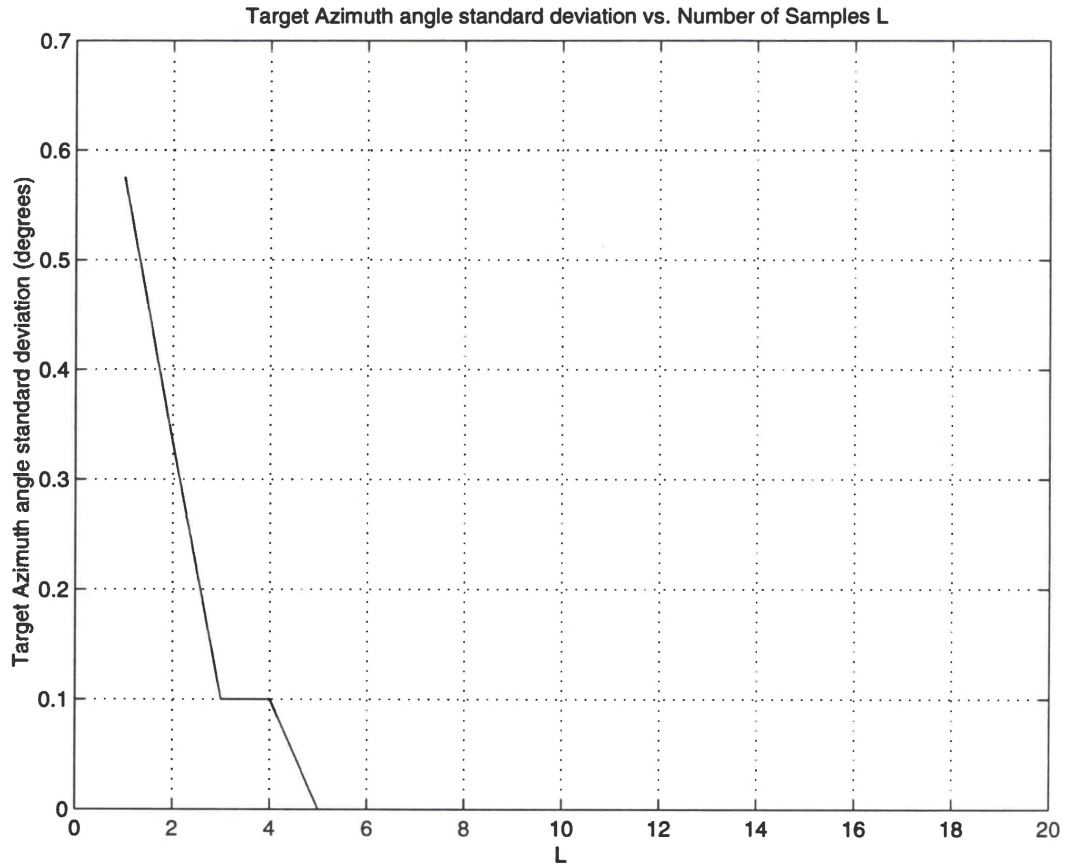**Figure 33.** Elevation standard deviation vs. L for $\xi d = 30$ dB, $\alpha d = \varepsilon d = 1$, and no jamming. Curve is computed from 100 trials.

Figure 34. Elevation standard deviation vs. L for $\xi d = 30$ dB, $\alpha d = \varepsilon d = 1$, and no jamming. Curve is computed from 400 trials.
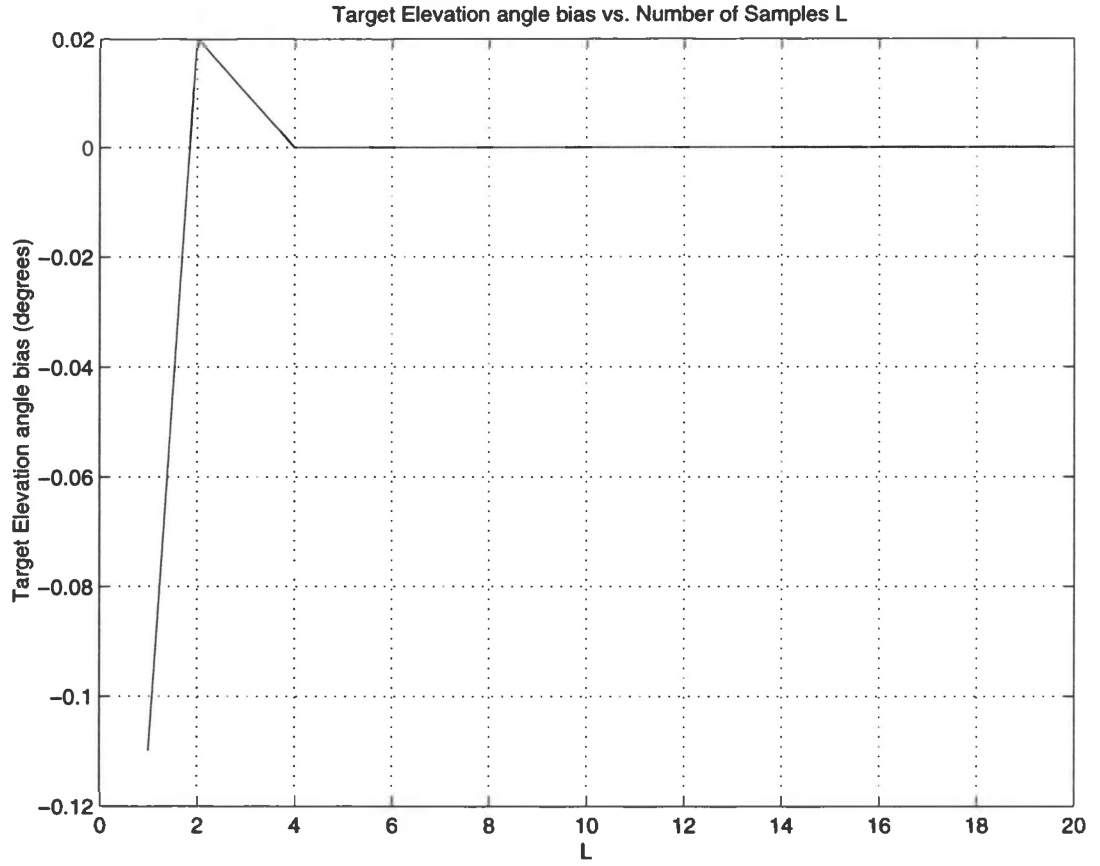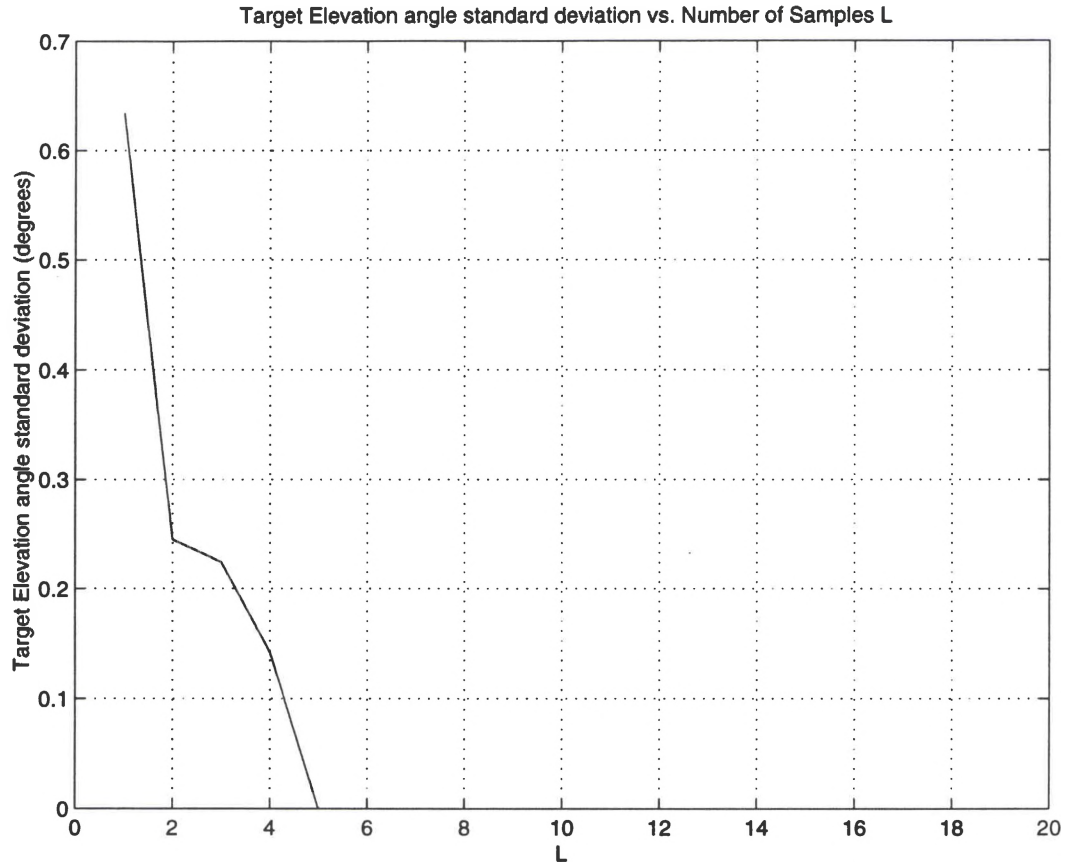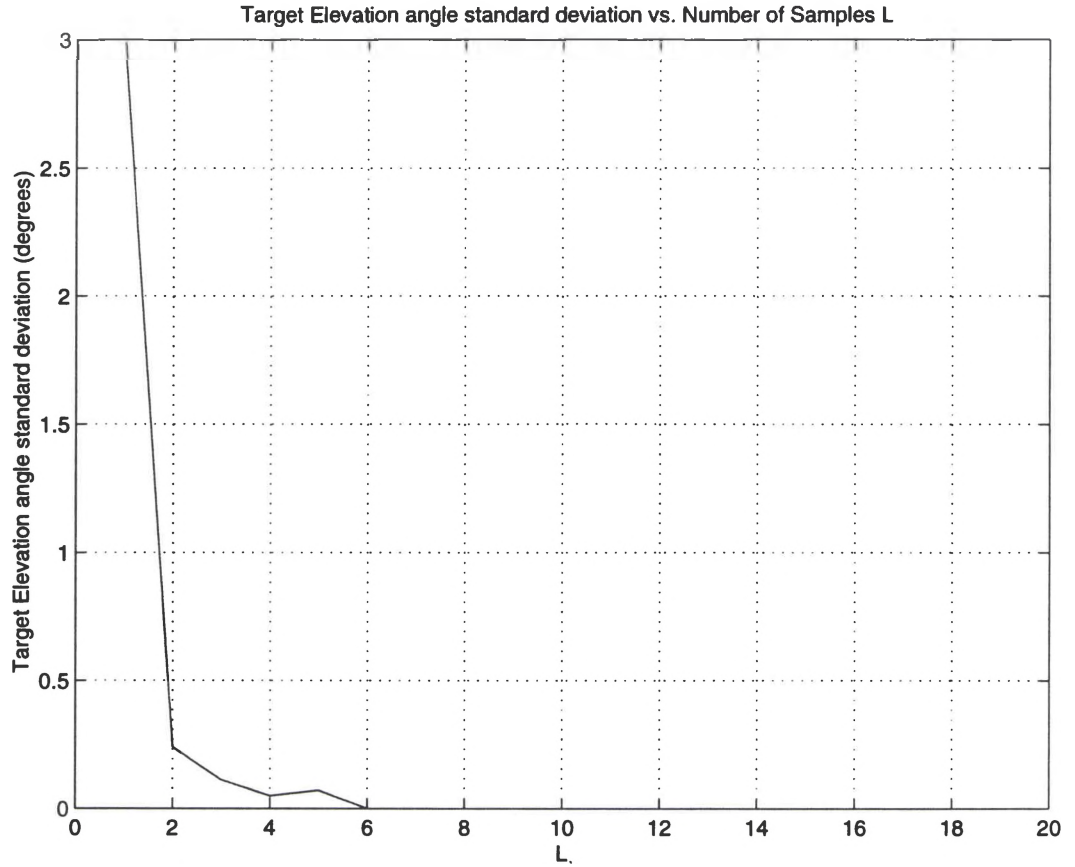
4.3 The Effect of Jamming

Now we will introduce jamming and examine its effects on the system. Figures 35-38 show the biases and standard deviation of α_d and ε_d as functions of the SNR when the desired signal arrives from $\alpha_d = \varepsilon_d = 1^o$ and a jammer arrives from $\alpha_j = \varepsilon_j = 30^o$ with a JNR of $\xi_j = 40$ dB. Figures 35-38 are computed from 100 trials with L = 8. Comparing these curves with Figures 22-25 shows that the jamming causes two changes:

(1) a higher SNR is required to reduce the bias to zero

(2) the standard deviation of α_d and ε_d is increased by more than an order of

magnitude.

Figure 35. Azimuth bias vs. SNR for $\alpha d = \varepsilon d = 1$, $\xi j = 40$ dB, $\alpha j = \varepsilon j = 30$ and $L = 8$. Curve is computed from 100 trials.

Figure 36. Azimuth standard deviation vs. SNR for $\alpha d = \varepsilon d = 1$, $\xi j = 40$ dB, $\alpha j = \varepsilon j = 30$ and L = 8. Curve is computed from 100 trials.

Figure 37. Elevation bias vs. SNR for $\alpha d = \varepsilon d = 1$, $\xi j = 40$ dB, $\alpha j = \varepsilon j = 30$ and $L = 8$. Curve is computed from 100 trials.
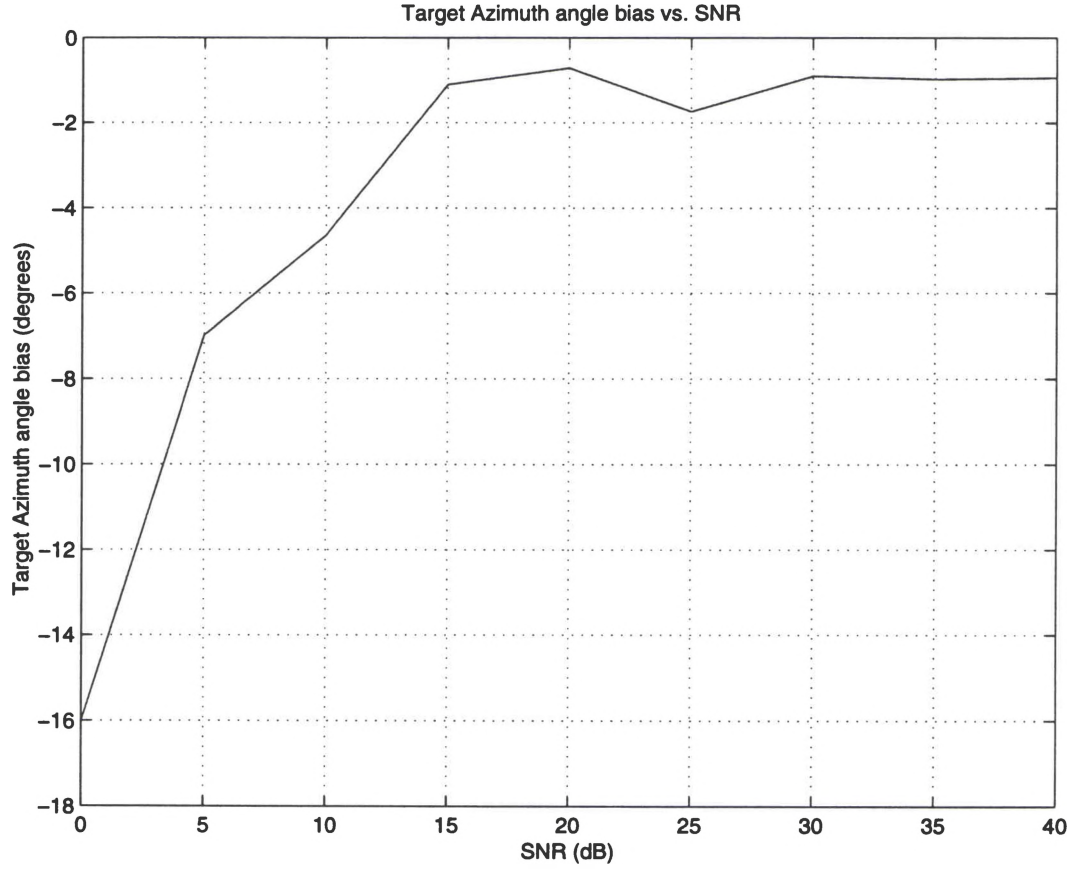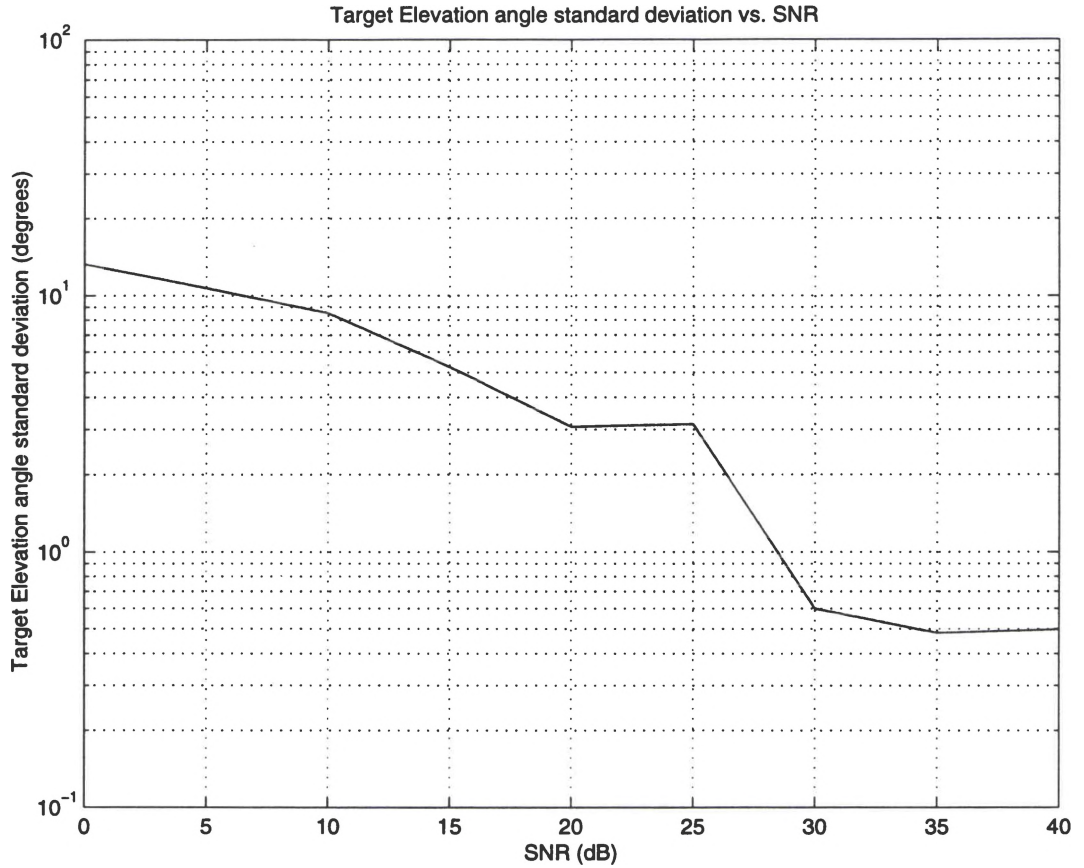
Figure 38. Elevation standard deviation vs. SNR for $\alpha d = \varepsilon d = 1$, $\xi j = 40$ dB, $\alpha j = \varepsilon j = 30$ and $L = 8$. Curve is computed from 100 trials.

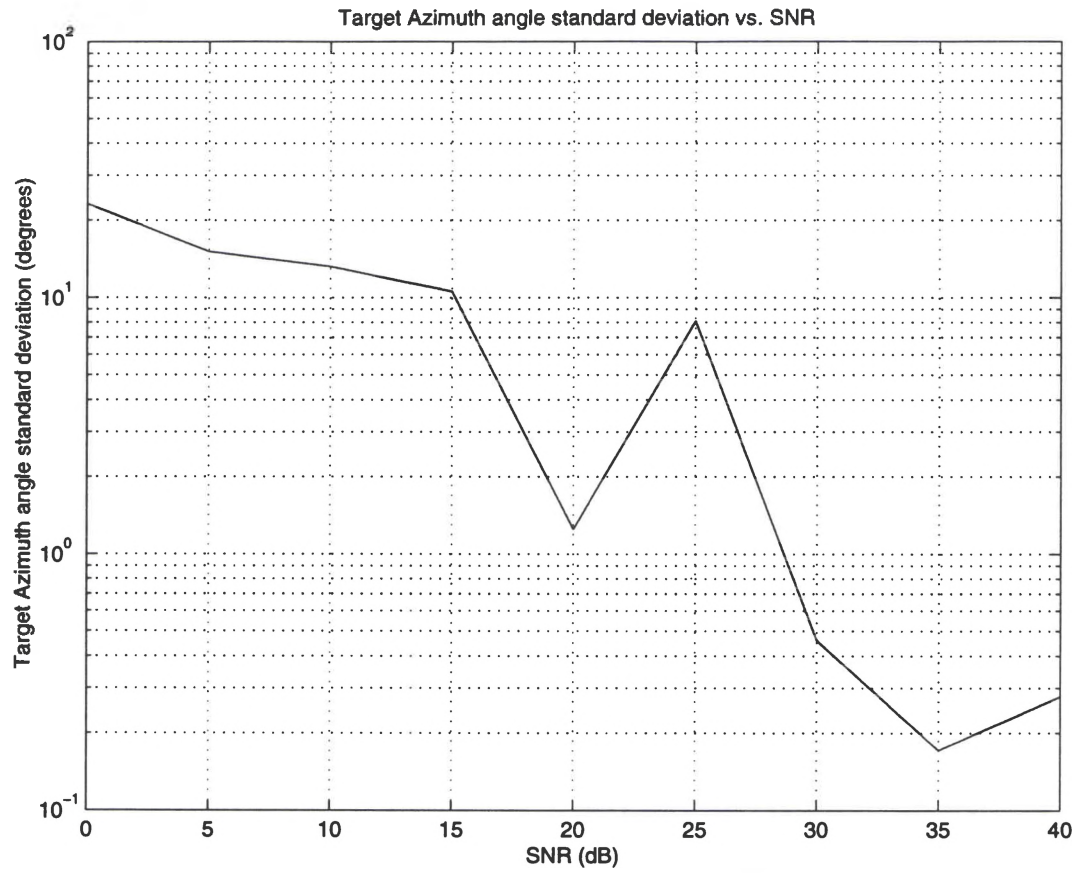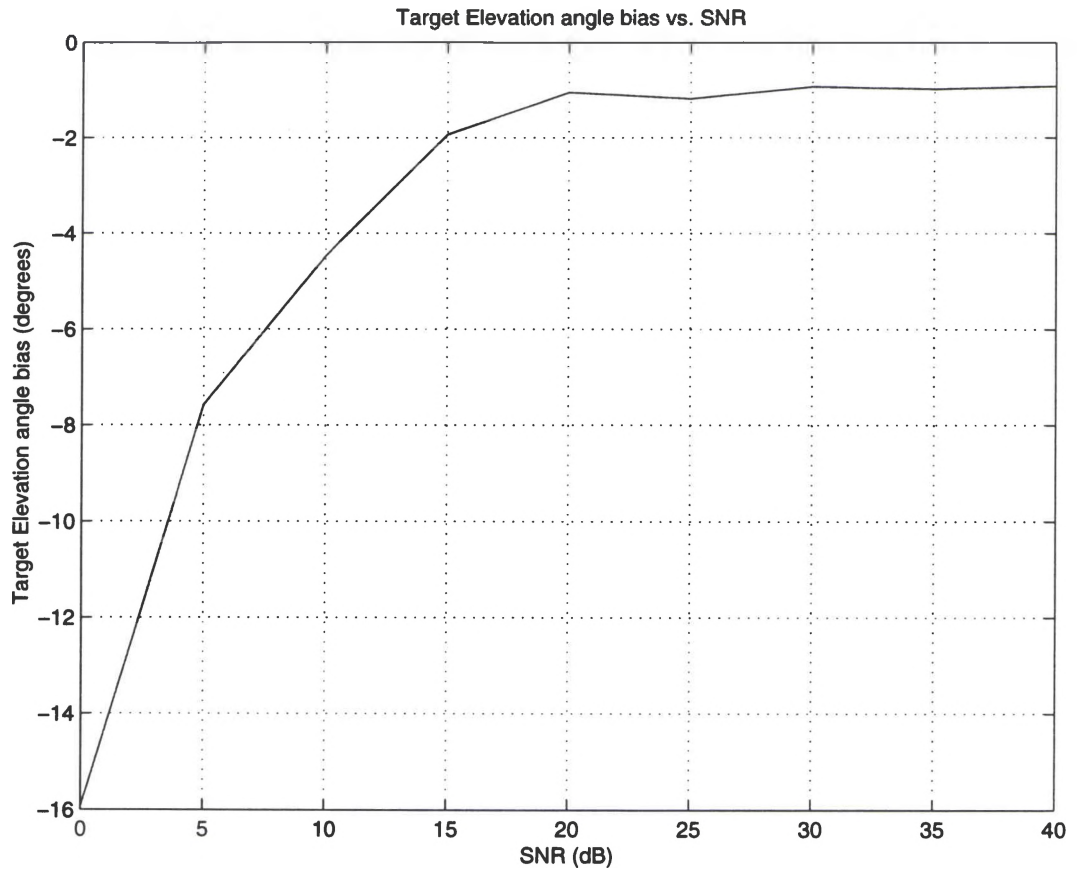## 4.4 The Effect of JNR

Figures 39-42 show the biases and standard deviations of α_d and ε_d as functions of the JNR when the SNR is $\xi_d = 30$ dB, $\alpha_d = \varepsilon_d = 1^o$, $\alpha_j = \varepsilon_j = 30^o$. One hundred trials are averaged with $L = 8$. There is a curious jump in the angle bias, Figures 39 and 41, at JNR = 25 dB most notable in elevation but also in azimuth. The largest change seems to occur between a JNR of –20 dB to 20 dB. We do not know the reason for this curious behavior.

Figure 39. Azimuth bias vs. JNR for $\xi d = 30$ dB, $\alpha d = \varepsilon d = 1$, $\alpha j = \varepsilon j = 30$ and $L = 8$. Curve is computed from 100 trials.
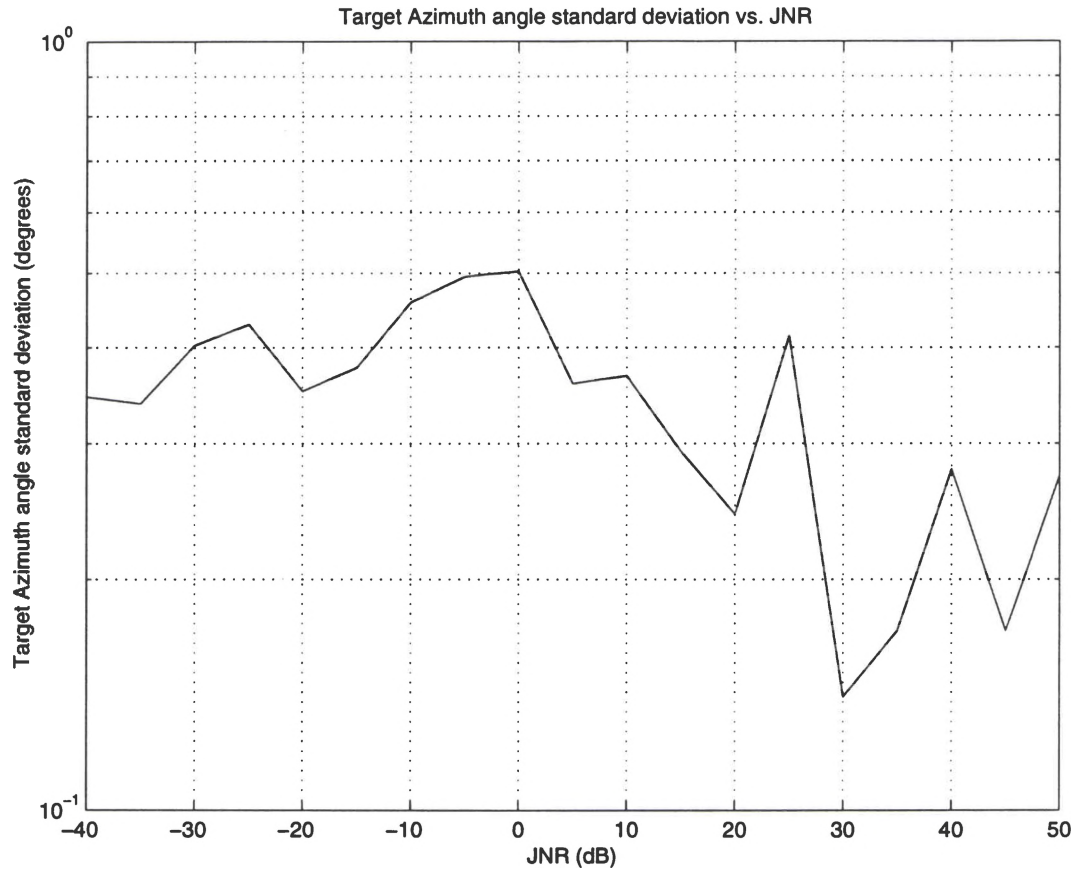
Figure 40. Azimuth standard deviation vs. JNR for $\xi d = 30$ dB, $\alpha d = \varepsilon d = 1$, $\alpha j = \varepsilon j = 30$ and L = 8. Curve is computed from 100 trials.
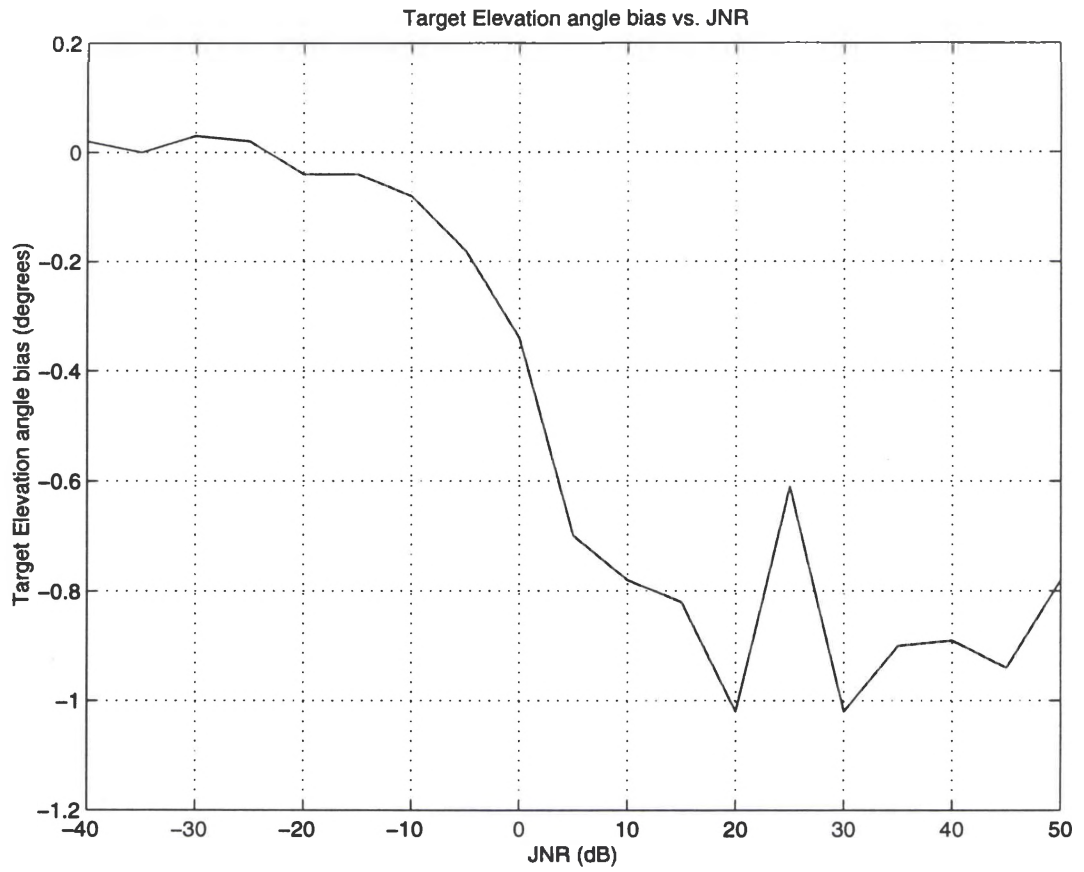
Figure 41. Elevation bias vs. JNR for ξd = 30 dB, αd = εd = 1, αj = εj = 30 and L = 8. Curve is computed from 100 trials.
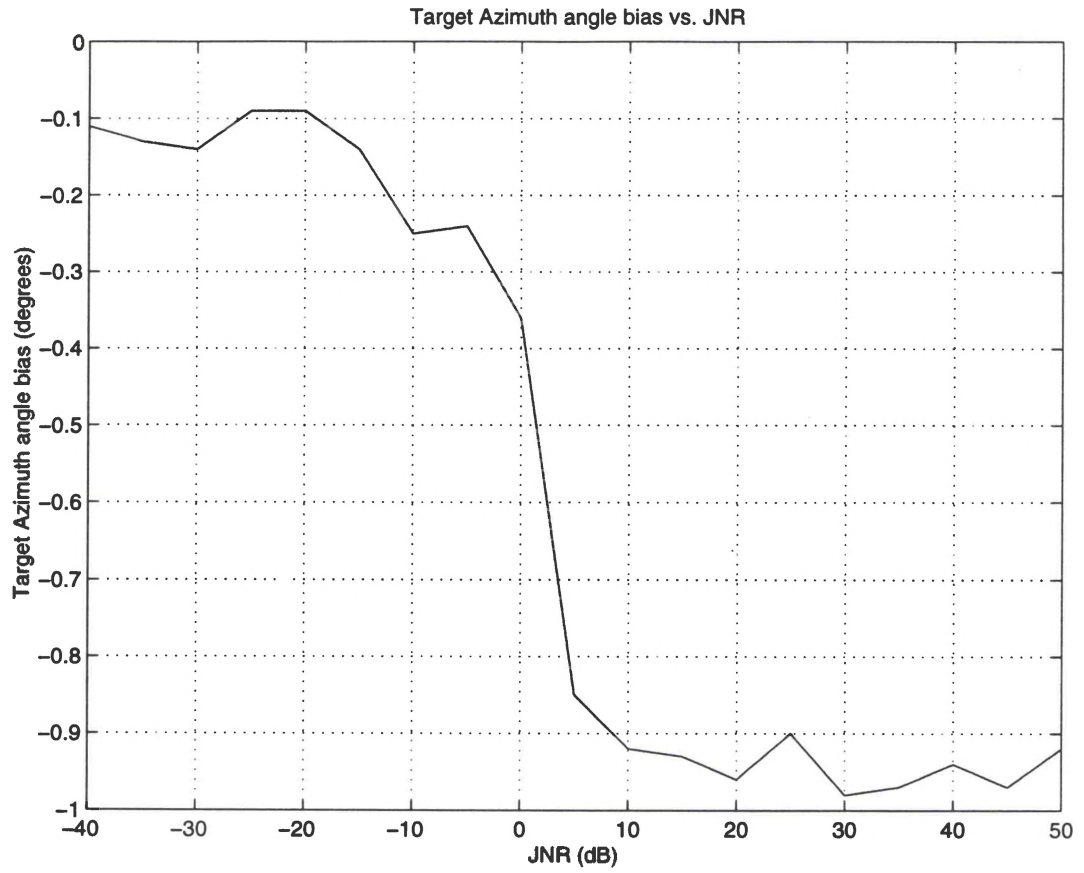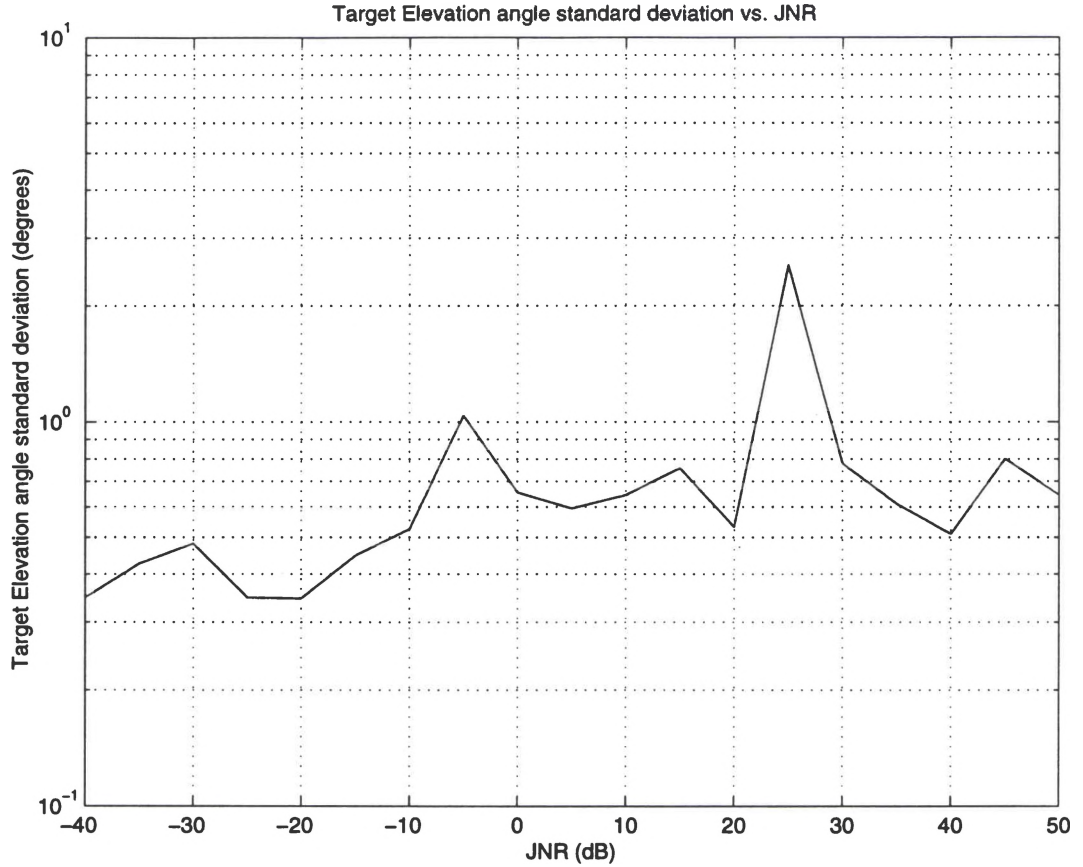
Figure 42. Elevation standard deviation vs. JNR for $\xi d = 30$ dB, $\alpha d = \varepsilon d = 1$, $\alpha j = \varepsilon j = 30$ and $L = 8$. Curve is computed from 100 trials.

4.5 The Effect of Target Position

The bias and standard deviation of α_d and ε_d as the desired signal azimuth angle α_d is

varied over the range are shown in Figures 43-46. 100 trials were averaged with $L = 8$.

Figures 43-46 show that the bias and the standard deviation of both α_d and ε_d are

considerably small to zero at $\alpha d = \varepsilon d = 0$ and increase dramatically as α_d approaches α_j.

This occurs because the peak of the P-surface is pulled away from the correct desired

signal angle due to incomplete jammer nulling and noise variations. This causes a high

standard deviation in the estimates. A similar problem occurs when ε_d is near ε_j.
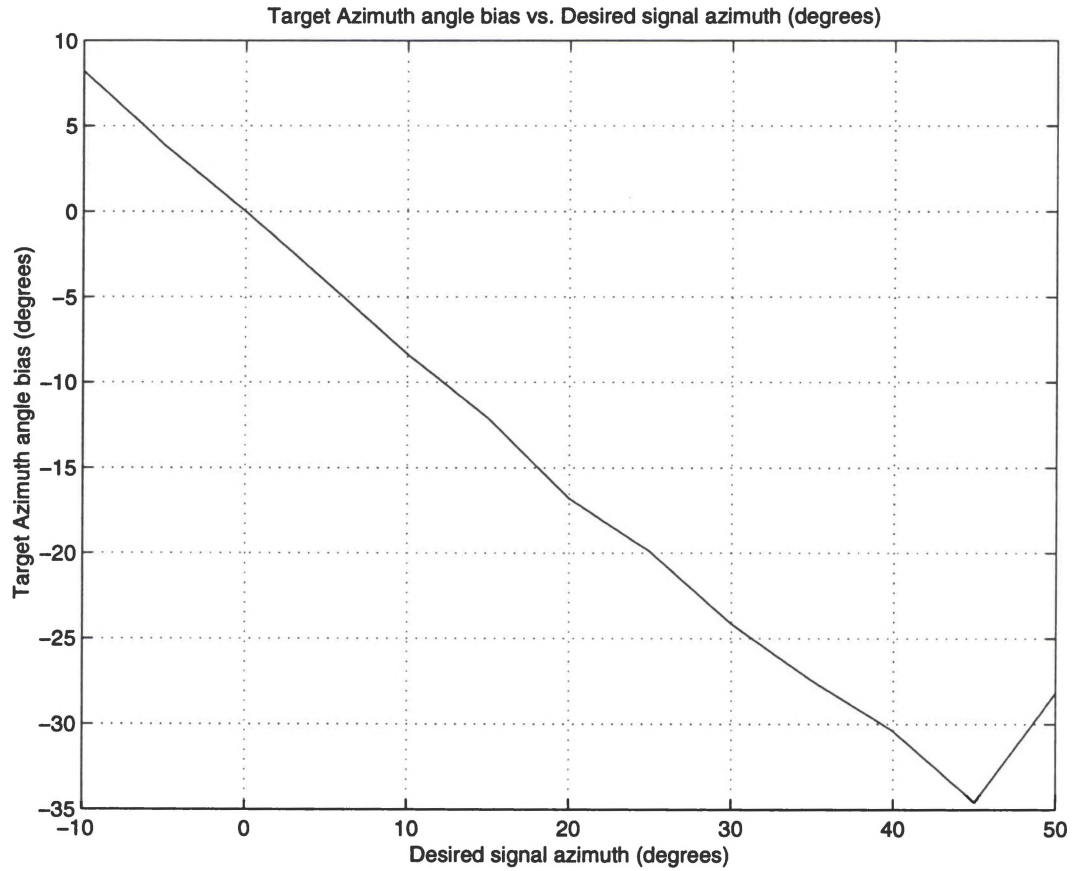
Figure 43. Azimuth bias vs. αd for $\xi d = 30$ dB, $\varepsilon d = 1$, $\xi j = 40$ dB, $\alpha j = \varepsilon j = 30$ and $L = 8$. Curve is computed from 100 trials.

Figure 44. Azimuth standard deviation vs. αd for $\xi d = 30$ dB, $\varepsilon d = 1$, $\xi j = 40$ dB, $\alpha j = \varepsilon j = 30$ and $L = 8$. Curve is computed from 100 trials.

Figure 45. Elevation bias vs. αd for ξd = 30 dB, εd = 1, ξj = 40 dB, $\alpha j = \varepsilon j$ = 30 and L = 8. Curve is computed from 100 trials.
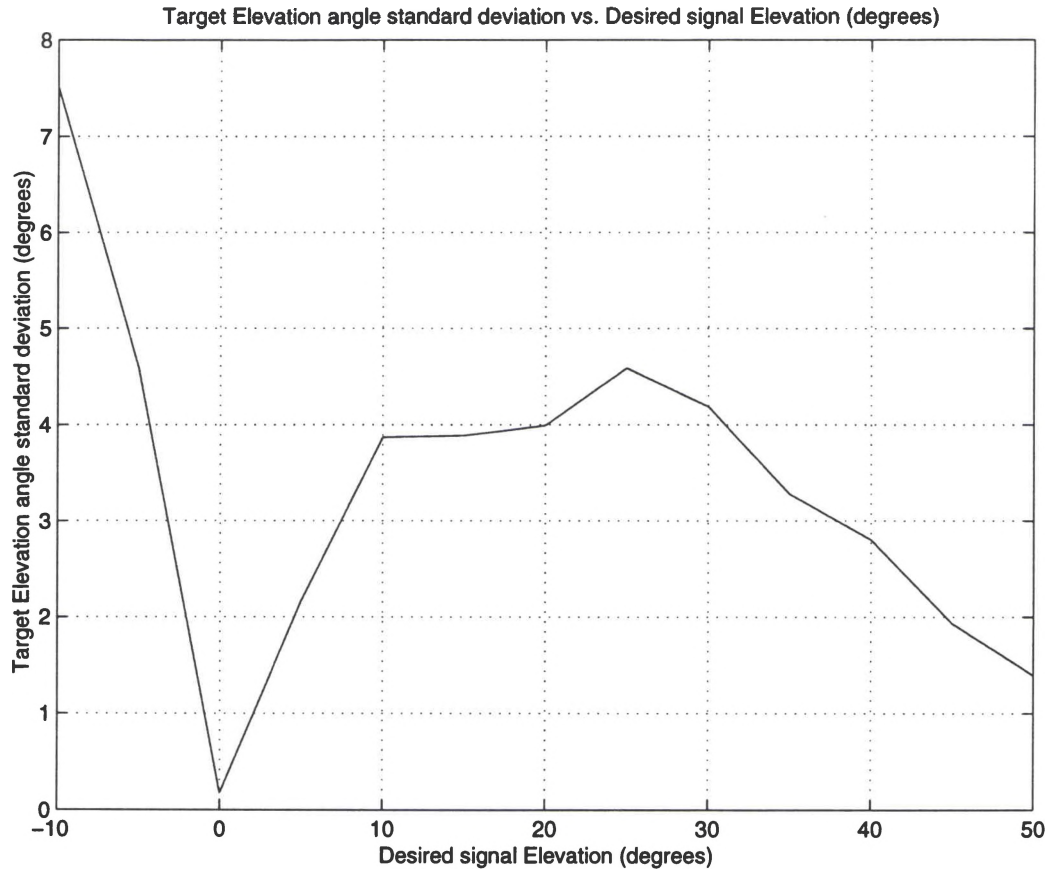
Figure 46. Elevation standard deviation vs. αd for $\xi d = 30$ dB, $\varepsilon d = 1$, $\xi j = 40$ dB, $\alpha j = \varepsilon j = 30$ and L = 8. Curve is computed from 100 trials.
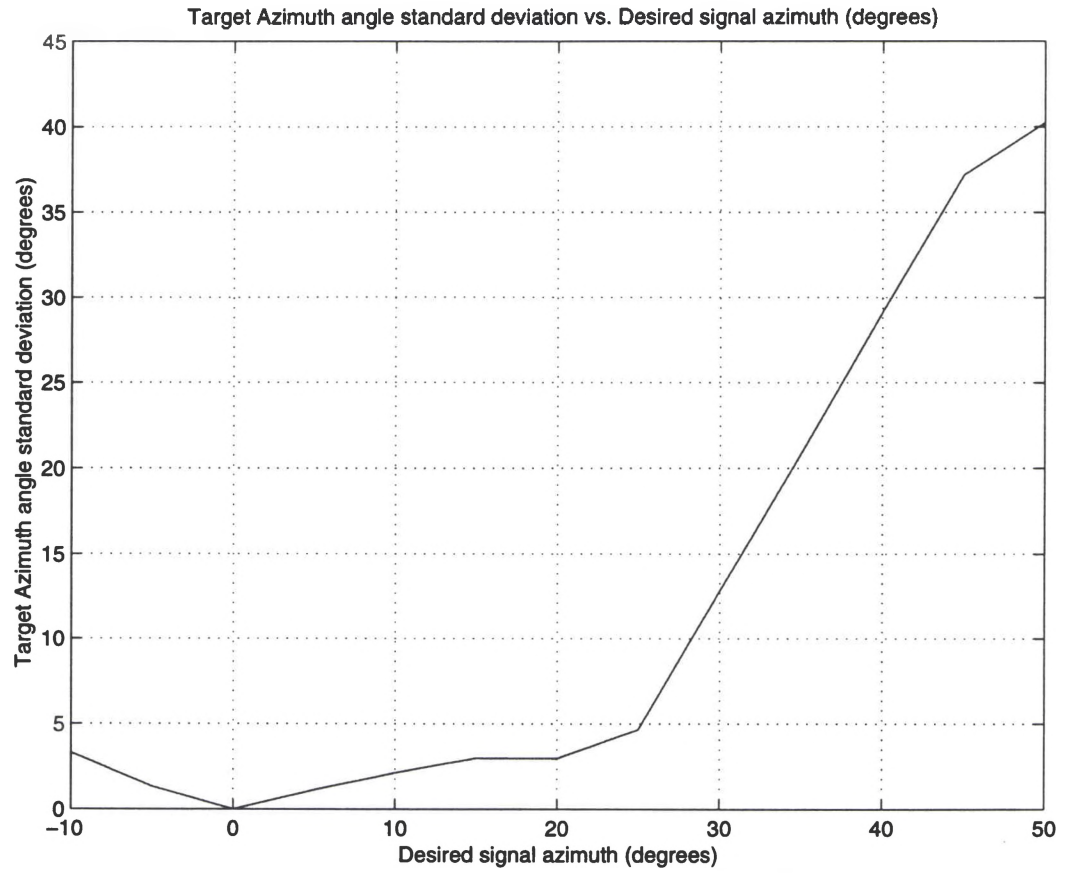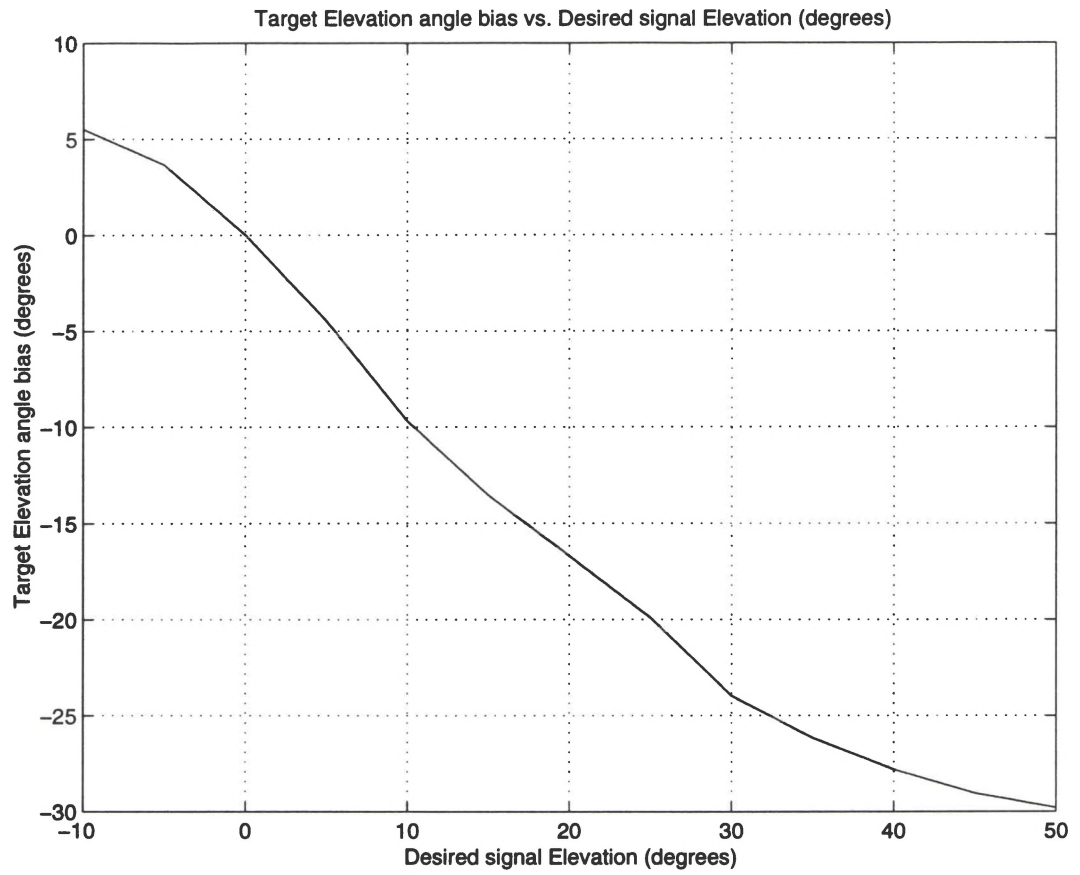
CHAPTER 5

CONCLUDING REMARKS

5.1 General Remarks

This thesis devised a new adaptive technique to estimate the azimuth and elevation angles of the target in the presence of a main lobe jammer and using a monopulse configuration. In the absence of main lobe jammer the monopulse system works very well, but the jammer tends to destroy the monopulse characteristic and the system fails completely. A number of efforts, for instance, Nickel [12], sought to develop corrections for the slope and zero crossing of the adapted monopulse ratio in the presence of jamming. Toulgor and Turner [13] also seek to eliminate the jammer component from the signal as was the case in the approach presented in this thesis but use a different method. They estimate the jammer subspace and then project the data to a space orthogonal to the jammer subspace to eliminate jammer component. MUSIC, suitably modified is then used to estimate the angle of arrival. The technique reported in this thesis consists of the following steps:

i)   The jammer component in each beam is eliminated by one of the other difference beams as an "auxiliary beam" and is subtracted.

ii)   The monopulse output, cleaned so to speak of the jammer component is then used to estimate the angle of arrival using the MUSIC algorithm.

iii)   The pseudo spectrum of the MUSIC algorithm reveals peaks corresponding to both the target and the jammer. The discrimination between the two peaks is made based on the signal power associated with their peaks, which is determined using least squares technique. The peak with the largest power is declared to be the target signal peak.

An extensive study based on MATLAB Simulation suggests that this angle estimator gives results comparable to that obtained using the deterministic Maximum Likelihood Method [6], [17]. However, locating the peaks is much simpler using the present method. The MLM approach requires the location of the maximums of a two dimensional surface which assumes very complex shapes in the presence of jamming.

5.2 Discussion of the Results

This thesis has examined the statistical performance of an adaptive monopulse MUSIC angle estimator operating with an array of four isotropic antenna elements. A target signal and a jamming signal are incident on the antenna, and each element signal also contains thermal noise. The estimator determines the azimuth and elevation angles of the desired signal. Monte Carlo trials have been run using a MATLAB simulation to determine the bias and standard deviation of the angle estimates as functions of the signal parameters.

Part 1 of Chapter 4 showed how the estimator performance is affected by the desired signal SNR. Also, results obtained from 100 Monte Carlo trails were compared to those obtained from 400 trials, in order to see the differences in the computed statistics. Part 2 examined the effect of L, the number of signal vectors combined to form the sample covariance matrix, on the estimator biases and standard deviations. Most of the curves in this thesis were obtained by using L = 8 (twice the number of adaptive channels). Part 3

of Chapter 4 showed that the presence of a jammer has two main effects. First, it increases the standard deviation of the estimates by more than an order of magnitude. Second, when jamming is present, a higher SNR is required to reduce the biases to zero. Part 4 of Chapter 4 showed how the JNR affects the estimator performance.

Part 5 of Chapter 4 examined how the estimator performance changes as the desired signal azimuth angle is scanned through the jammer azimuth angle.

The results show that the estimation by both the MLE and the MUSIC algorithm are similar. The main difference is shown in Figure 47, where the plane around the detection space is more complex with the MLE estimator. Note that the MUSIC algorithm generates a narrow, large peak at the estimation angle. In the case of jamming, the MUSIC algorithm outperforms the standard MLE algorithm in that the jamming-MLE peak exhibits a complex surface geometry around the estimated angle.
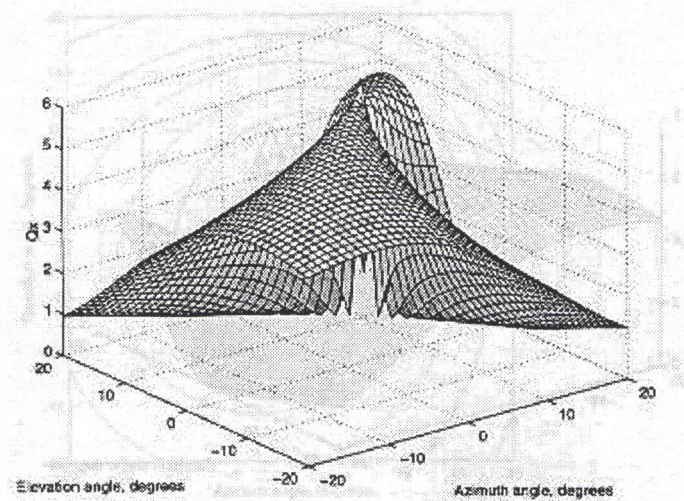

Figure 47. MLE Q surface for $\xi_d = 30$ dB, $\varepsilon_d = 1$, $\xi_j = 40$ dB, $\alpha_j = \varepsilon_j = 30$ and L = 8. Courtesy of [17]

5.3 Contributions to State-of-the-Art

As stated earlier, the main contributions of the thesis are that the MUSIC algorithm performs as well as the maximum likelihood estimator. However the location of the target from the MLE suffers from a complex geometry, whereas the MUSIC algorithm generates a simple geometrical surface. The simplicity of the space is needed for further processing since the gradient of the measurement can give additional information such as the confidence of the measurement. For instance, if the gradient is large, or the beam-width is small, then the detection of the angle estimation of azimuth and elevation is high.

5.4 Future Work

There are many issues to further explore in the implementation of the MUSIC algorithm. Such examples of the extension of the work include: real data, theoretical limitations of the algorithm, moving targets with varying angles, integrated measurements with other sensors such as Inertial Navigation Systems (INS) [19] and the integration of the MLE with the MUSIC algorithm. It is hoped that some of these issues will be resolved in the dissertation. Additionally, such issues as learning might be extended with this work [20].

There are a number of issues that could not be addressed in the present investigation but deserve to be examined. Some of these are listed below:

i) The element patterns constituting the monopulse system are taken to be isotropic. In a real system, they actually would be a large array, with a relatively narrow beam. The effect of such a pattern must be taken into account.

ii) In formulating the MUSIC Signal Model, the steering vectors are affected by the adapted weights. However, this is not taken into account in computing the

MUSIC pseudo spectrum. It would be interesting to modify the steering vectors appropriately to compute the MUSIC spectrum.

iii) Monopulse yields best results when the target is at the boresight. Once an estimate of the target is obtained, it is possible to steer the monopulse system so that the target is close to the boresight and then process the data again to compute an updated estimate. It is expected that this estimate would have better statistical properties than the earlier estimate.

REFERENCES

[1] Van Trees, H. L., *Detection, Estimation, and Modulation Theory*, John Wiley and Sons, Inc., New York, NY, 1968.

[2] Miller, M. I. And D.R.Fuhrman, 'Maximum-likelihood narrow-band direction finding and the EM algorithm,' *IEEE Transactions on Acoustics, Speech, and Signal Processing*, Vol. 28, no. 9 (Sept 1990). pp.1560-1577.

[3] Pillai, S. U. *Array Signal Processing*, Springer-Verlag., New York, NY, 1989.

[4] Ziskind, I., and M Wax, 'Maximum-likelihood localization of multiple sources by alternating projection,' *IEEE Transactions on Acoustics, Speech, and Signal Processing*, Vol. ASSP-36, no. 10 (Oct 1988). pp.1553-1560.

[5] Stoica, P, and A. Nehorai, 'Performance study of conditional and unconditional direction-of-arrival estimation,' *IEEE Transactions on Acoustics, Speech, and Signal Processing*, Vol 38, no 10 (Oct 1990), pp. 1783-1795.

[6] Compton, R.T., 'Adaptive Maximum Likelihood Angle Estimate Bias with a monopulse antenna under ideal conditions,' Tech Report WL-TR-97-1148, Wright Laboratory.

[7] Brennan, Reed and Davis, 'Parameter estimation of superimposed signals using the EM algorithm,' . *IEEE Transactions on Acoustics, Speech, and Signal Processing*, Vol. ASSP-36, no. 4 (Apr 1988). pp. 477-489.

[8] Feder, M. and E. Weinstein, 'Parameter estimation of superimposed signals using the EM algorithm,' . *IEEE Transactions on Acoustics, Speech, and Signal Processing*, Vol. ASSP-36, no. 4 (Apr 1988). pp. 477-489.

[9] Roy, R. and T. Kailath., 'ESPIRIT - Estimation of signal parameters via rotational invariance techniques,' *IEEE Transactions on Acoustics, Speech, and Signal Processing*, Vol. ASSP-37, no. 7 (July 1989), pp. 984-995.

[10] Lin, Feng-Ling C. and Kretschmer, Frank F., 'Angle Estimation in the presence of Mainbeam Interference,' NRL Report 9234 AD-A216 832 (December 1989).

[11] Theil, 'Angle Estimation in the presence of Mainbeam Interference,' NRL Report 9234 AD-A216 832 (December 1989).

[12] Nickel, U., 'Monopulse Estimation with Adaptive Arrays,' IEE Proceedings-F, Vol. 140, No. 5, (October 1993) pp. 303-308.

[13] Toulgoat, Mylene and Turner, Ross M., 'Estimation of Target Angular Position Under Mainbeam Jamming Conditions,' Defence Research establishment Ottawa, Report No. 1281 (December 1995).

[14] Schmidt, R. O., 'Multiple emitter location and signal parameter estimation,' *IEEE Transactions on Antennas and Propagation*, Vol. AP-34, no. 3 (Mar 1986), pp. 276-280.

[15] Morris, Guy V., 'Airborne Pulsed Doppler Radar,' ARTECH HOUSE, INC., (1988)

[16] Stimson, George W., 'Introduction to Airborne Radar,' Hughes Aircraft Company (Mar 1983)

[17] Compton, R.T., 'The Statistical Performance of Adaptive Maximum Likelihood Angle Estimation with a Simple Monopulse Antenna,' Tech Report WL-TR-97-1149, Wright Laboratory.

[18] Reed, L.S., Mallett, J.D., and Brennan, L.E.,'Rapid Convergence Rate in Adaptive Arrays,' *IEEE Transactions*, Vol. AES-10, No. 6 (November 1974), pp. 853-864.

[19] Layne, J, R. and E. Blasch, 'Integrated Synthetic Aperture Radar and Navigation Systems for Targeting Applications,' Tech Rep. WL-TR-97-xxx, Wright Laboratory, Wright Patterson AFB, Ohio, October 1997.

[20] Johnson, J, H. Li, E. Culpepper, E. Blasch, and A. Klopf, 'Learning Algorithms for Suppressing Motion Clutter in Airborne Array Radar,' *National Aerospace and Electronics Conference*, Dayton, Ohio, July 1997, pp. 840-845.

VITA

Edwin Culpepper was born on 3 July 1962 in Cleveland, OH. He graduated from Lutheran High School East in 1980 and attended the University of Evansville in Indiana, graduating with a Bachelor of Science degree in Electrical Engineering. He also co-oped with Wright-Patterson AFB near Dayton, OH during his undergraduate studies. Since then, he has been a full-time employee at Wright-Patterson, currently assigned to the Targeting and Attack Radar Branch of the Sensors Directorate for the Air Force Research Laboratory while earning a Master of Science degree in Electrical Engineering at the University of Dayton. Mr. Culpepper's area of expertise is in adaptive and array signal processing for radar and communications.